MICROWAVE OPTICS USING DIELECTRIC PRISMS AND DIELECTRIC RODS

MICROWAVE OPTICS USING DIELECTRIC PRISMS AND DIELECTRIC RODS

By

MUHAMMAD ZAHUR ALI, B.Sc. (Hons.), M.Sc. (Dacca)

A Thesis

Submitted to the Faculty of Graduate Studies

in Partial Fulfilment of the Requirements

for the Degree

Master of Science

McMaster University

October 1966

MASTER OF SCIENCE (1966)
(Physics)

McMASTER UNIVERSITY
Hamilton, Ontario

TITLE: Microwave Optice Using Dielectric Prisms and Dielectric Rods

AUTHOR: Muhammad Zahur Ali

SUPERVISOR: Professor A. B. McLay

NUMBER OF PAGES: viii, 65 (including 21 figures)

ABSTRACT

The effects of two types of prisms on the standing wave patterns and on the radiation field patterns have been investigated. It is shown that the boundary faces of the dielectric prism behave as the boundary walls of a dielectric waveguide and concentrate the power at the tip of the prism.

An effort was made to investigate the Goos-Haenchen shift inside the waveguide. It was not possible to observe any Goos-Haenchen shift inside the waveguide.

Diffraction patterns have been studied with the electric vector perpendicular to the axis of two dielectric rods of two different diameters (a = 1.916 cm, 1.233 cm). Runs have been taken across and along the direction of propagation of the beam. Some experimental results have also been compared with the calculated results.

ACKNOWLEDGEMENTS

I wish to express my sincere thanks and gratitude to Dr. A. B. McLay for his guidance and advice throughout the course of this research project.

I wish to thank Dr. M. W. Johns for his advice and suggestions in many matters.

I wish to thank Dr. C. V. Stager and Dr. T. Timusk for their generous help and criticism during the writing of this thesis.

It is a pleasure to thank my friends, Mr. H. C. Bezner and Mr. L. A. A. Read, for their co-operation, understanding and help in many ways.

I wish to express my appreciation to Mr. M. Afsar for helping me with the drawing of some of the figures.

Finally, I would like to thank the Colombo Plan Authority in Ottawa for making financial and other arrangements.

TABLE OF CONTENTS

LIST OF FIGURES

CHAPTER 1

INTRODUCTION

1-1 Microwaves

The whole of the electromagnetic spectrum can be separated into two parts according to the processes of generation and detection. The first region can be called the "Quantum Region" which extends from cosmic radiation of shortest wavelength through X-rays, visible radiation, infrared and finally into the far-infrared region. In this whole region, the process of generation of radiation involves a transition between energy states of a particle of atomic or nuclear dimensions and, therefore, the fundamental process of generation of radiation is usually discrete.

The second region, called the "Radio Region", is associated with the radiation of longer wavelengths. Here, the frequency of radiation can be controlled by the shape and size of electrical circuits and can be detected by transforming the radio frequency energy into some form of mechanical motion, e.g. deflection of a meter. The short wavelength region of the radio-spectrum, adjacent to the far-infrared region, is known as the microwave region.

The boundaries of the microwave spectrum are not sharply defined since the processes of generation and detection of microwaves may also be used to some extent in the overlapping regions. However, today the region of wavelengths between 1 mm and 50 mm is identified

as the microwave region. For practical purposes, the microwave region has been subdivided into several bands. The present experimental studies are carried out in the X-Band (3.75 cm - 2.50 cm) region.

1-2 Microwave Optics

In principle, diffraction can be associated with the whole of the electromagnetic spectrum. In any region of the spectrum, one may distinguish two cases: (1) The ratio of obstacle dimension to the wavelength of radiation is less than one. (2) The ratio of obstacle dimension to the wavelength of radiation is of the order of one or more than one. The latter case may be most easily investigated by microwave techniques where the wavelength is comparable to the dimensions of laboratory apparatus. The domain of microwave optics can be distinguished by the following features:

(i) Microwave radiation shows full temporal and spatial coherence with definite polarization of the field, usually linear.

(ii) Diffraction effects are very much in evidence, since wavelengths are of the order of laboratory apparatus dimensions and, therefore, it is impossible to obtain an ideal plane microwave beam in the laboratory.

(iii) Measurement and detection methods, in the microwave region, make it possible to determine the actual electromagnetic fields. Optical techniques permit the measurements of only the mean quadratical quantities $\langle E^2 \rangle$ and $\langle H^2 \rangle$.

In "visible light optics", diffraction effects were known in the early part of the nineteenth century. Since the magnitude of diffraction effect is involved with the ratio of the obstacle dimension to the wavelength, diffraction using light is observable only very close to geometrical shadow edges at great distances beyond the diffracting object. Using visible light, it is practically impossible to observe diffraction effects at distances from the obstacle which are comparable with the wavelength.

Since 1940, the availability of microwave generating systems has permitted investigation of diffraction in the close vicinity of an obstacle or aperture. Much attention has been paid to this subject since 1950 when better detecting devices became available. Many people undertook experimental investigations in this field. In this regard, a particular mention must be made of the Cruft Laboratory (Harvard) where a considerable number of experiments on diffraction and scattering were conducted. For instance, C. H. Papas (1950) and R. D. Kodis (1952) observed microwave diffraction by cylindrical objects.

A complete and comprehensive theory for the diffraction of microwaves by dielectric cylindrical objects was first given by C. Froese and J. R. Wait (1954). Investigations of diffraction effects using microwaves have also been undertaken in this laboratory since 1950 and continued to the present day.

1-3 Development of Microwave Optics at McMaster University

Quite a considerable number of experiments have been done in

this microwave optics laboratory since 1950. D. B. McLay (1951) studied the diffraction of microwaves of 10 cm and 3 cm wavelengths by conducting rods and detected the intensities by the use of "dummy" half-wave dipoles. S. T. Wiles (1952) studied the diffraction patterns for a one-inch brass and a one-inch rubber rod with the electric vector parallel to the axis of the rod. His measurements included intensities and phases. Then J. E. Keys (1953) studied the diffraction of microwaves by brass, hard rubber and lucite cylinders using the polarization (E-component) perpendicular to the axis of the rod. The results of his experiments on a lucite cylinder were communicated to C. Froese and J. R. Wait (1954) who have compared the experimental results with their calculated results. M. K. Subbarao (1956) continued the studies of diffraction for the 1.0 inch and 1.5 inch rods of tenite and lucite materials and compared the experimental results with the calculated results for the theory by J. R. Wait (1954). In his experimental studies the electric component was parallel to the axis of the rod. M. K. Subbarao (1956) and C. E. Jordan (1957), with the same polarization, investigated the region close to a semi-cylinder with the plane-face towards and away from the source.

Investigations of diffractions by a large 45°-90°-45° dielectric prism and of evanescent waves have been carried out by different experimenters in this laboratory. Diffraction patterns for 45° and 90° wedges have been studied by C. E. Jordan (1957), R. Dignum (1960) and N. E. Hedgecock (1959) using various orientations of the 45°-90°-45° prism. The evanescent wave behind

a totally internally reflecting surface has been investigated by C. E. Jordan (1957), P. Leung (1961) and in detail by N. E. Hedgecock (1959). Then W. A. Young (1963) studied the intensity patterns along the direction of propagation of the beam behind circular brass and lucite, and semi-circular lucite rods with and without a foil cover. In his experimental studied, the electric vector was perpendicular to the axis of the rod.

1-4 Present Experimental Studies

The present experimental work consists of two parts, based on the two diffraction geometries that have been investigated in this laboratory, namely, the wedge diffraction by large prisms and diffraction by circular rods. The first part contains an investigation using small prisms and the second part contains an investigation using dielectric rods.

To study the diffraction by a prism, a prism was placed in a 3 cm waveguide and illuminated with 3 cm microwaves. Although the incident wave is more complicated than a plane wave in free space, it is well defined spatially. Both the reflected and transmitted waves can be investigated.

In another experiment, an investigation of the Goos-Haenchen shift was made. When an incident beam is totally reflected internally, the emergent beam is seen to be laterally displaced from the position predicted by geometrical optics (Fig. 1(a)). The displacement is of the order of a wavelength and is known as the Goos-Haenchen shift (Goos and Haenchen, 1947). Goos and Haenchen used visible light and

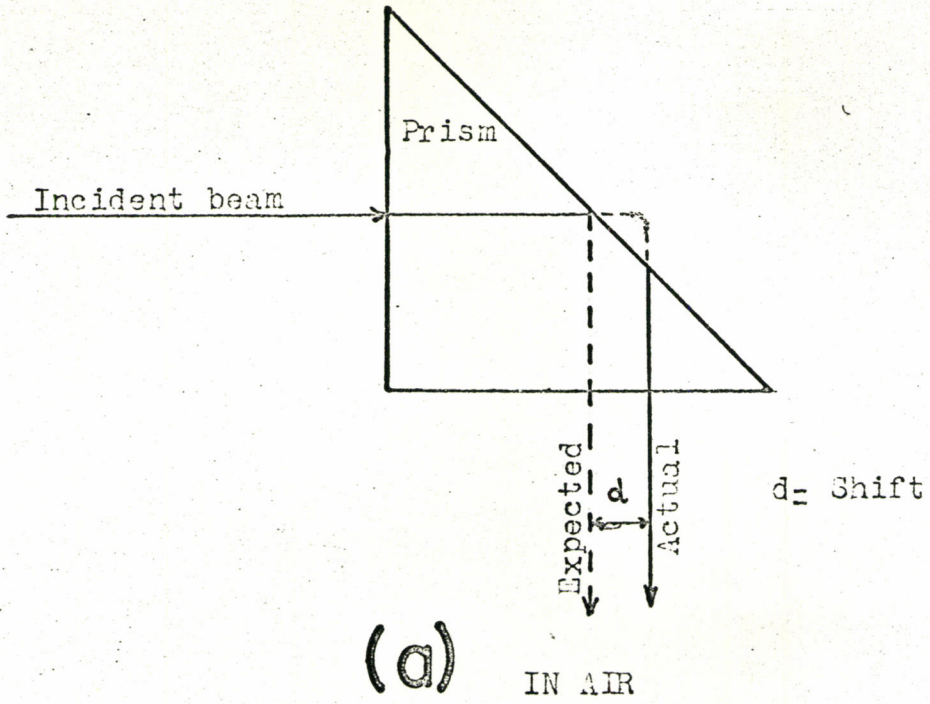

(a) IN AIR

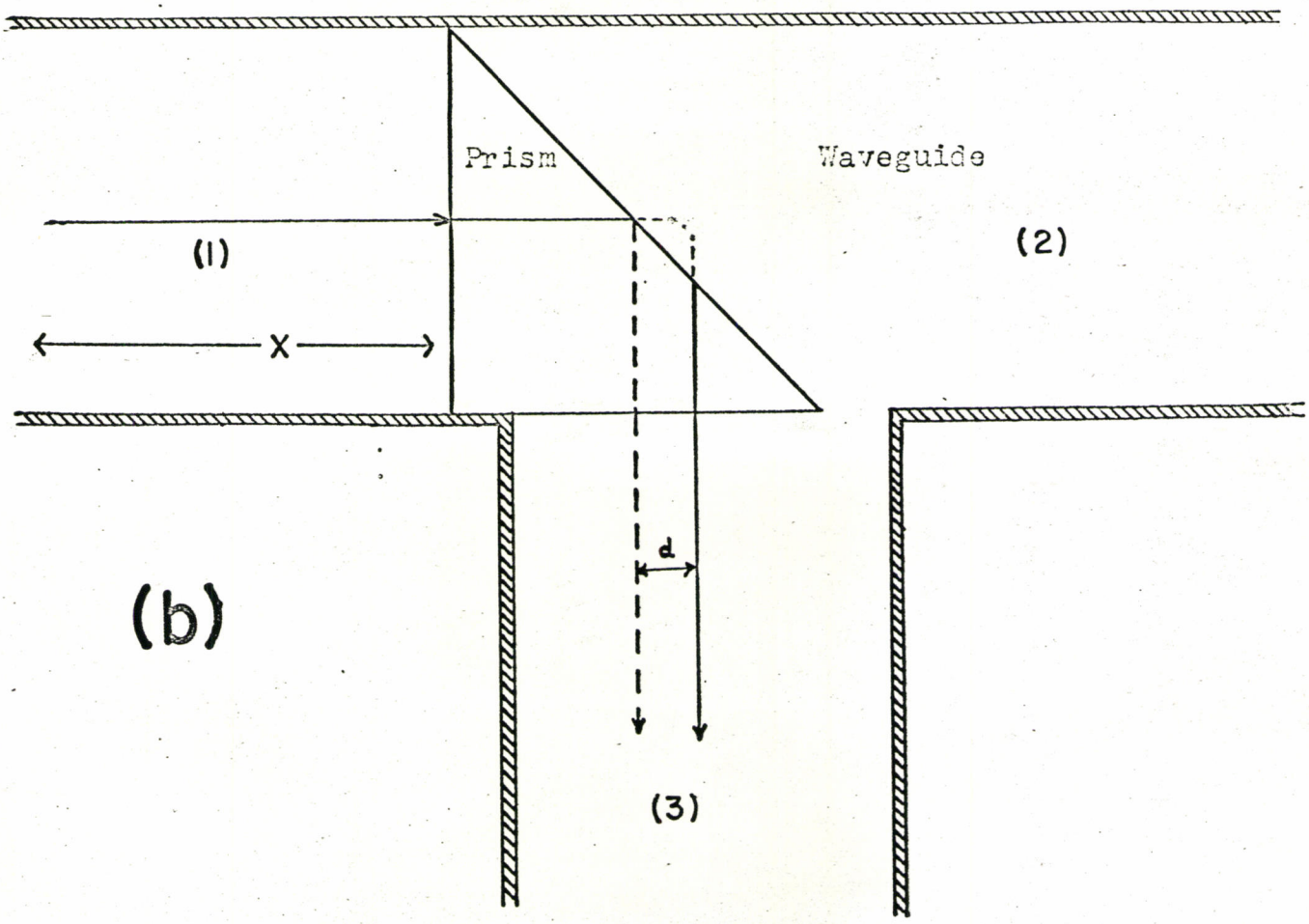

(b) IN WAVEGUIDE

FIG·1

the small shift made it necessary for them to use multiple reflections to obtain an observable shift. However, since microwave wavelengths are of the order of centimeters, a single total reflection is enough to show a measureable shift. In this experiment, the investigation of the Goos-Haenchen effect was undertaken with the prism inside a waveguide. H. C. Bezner is presently working on the Goos-Haenchen shift using microwaves in free space where the investigation is simpler.

The second part of the experimental investigation consists of diffraction of microwaves by lucite cylindrical rods. Diffraction with the electric vector parallel to the axis of the cylinder has been done fairly extensively in this laboratory. However, experiments with the electric vector perpendicular to the axis of the rod have not been as extensively studied because of the experimental difficulties with this polarization. The present diffraction experiment consists of cases where the runs were taken across as well as along the direction of propagation of the beam.

CHAPTER 2

THEORETICAL CONSIDERATIONS

2-1 Goos-Haenchen Shift

In 1943, Goos and Haenchen devised an experiment to show what happens at the total reflection if the incident wave penetrates into the medium of lower index and re-emerges into the medium of higher index. Their experiment confirmed the expected shift of the beam.

The cause of the shift is that for a finite incident plane wave suffering total internal reflection, on the average, some energy enters into the medium of lower index on one side of the beam (Fig. 1(a)) and comes back into the medium of higher index on the other side of the beam. The Goos-Haenchen shift is identified with a lateral translation of the beam. An expression for the Goos-Haenchen shift (Renard, 1964) for the perpendicular polarization is given by

$$d = \frac{1}{\pi} \times \frac{\mu \sin i \cos^2 i}{\mu^2 \cos^2 i + \sin^2 i - n^2} \times \frac{\lambda_1}{(\sin^2 i - n^2)^{\frac{1}{2}}} \qquad (2.1)$$

where,

$$n = \frac{n_2}{n_1} \quad (n_1 > n_2)$$

n_1, n_2 = refractive indices

$$\mu = \frac{\mu_2}{\mu_1}$$

μ_1, μ_2 = magnetic permeabilities

i = angle of incidence

$\lambda_1 = \frac{\lambda_o}{n_1}$

λ_o = free space wavelength.

A similar type of shift (Fig. 1(b)) might be expected with a prism inside the waveguide and therefore an experimental set up was made to investigate this effect.

2-2 Diffraction by a Dielectric Cylinder

The diffraction field around a dielectric cylinderical rod exhibits pronounced maxima and minima. Some of these effects could be explained crudely by geometrical optics, however, a complete quantitative description can only be found from a solution of the boundary value problem. This present theory is based on the paper by C. Froese and J. R. Wait (1955).

The geometry of the diffraction problem is shown in Fig. 2. S is the source of radiation, SX is the axis of propagation of the incident cylindrical wave symmetry and P is any arbitrary field point. O is the centre of the cylinder and Z is the axis of the rod normal to the plane of the diagram. The waves from S are considered cylindrical at the point P but in the close vicinity of the cylinder, the waves are considered plane as $a << OS$. We assume that a plane linearly polarized electromagnetic wave propagates along the X-axis and therefore the incident plane wave, when electric vector Ey is perpendicular to the axis of the cylinder, can be written in the form,

GEOMETRY OF DIFFRACTION BY CIRCULAR RODS

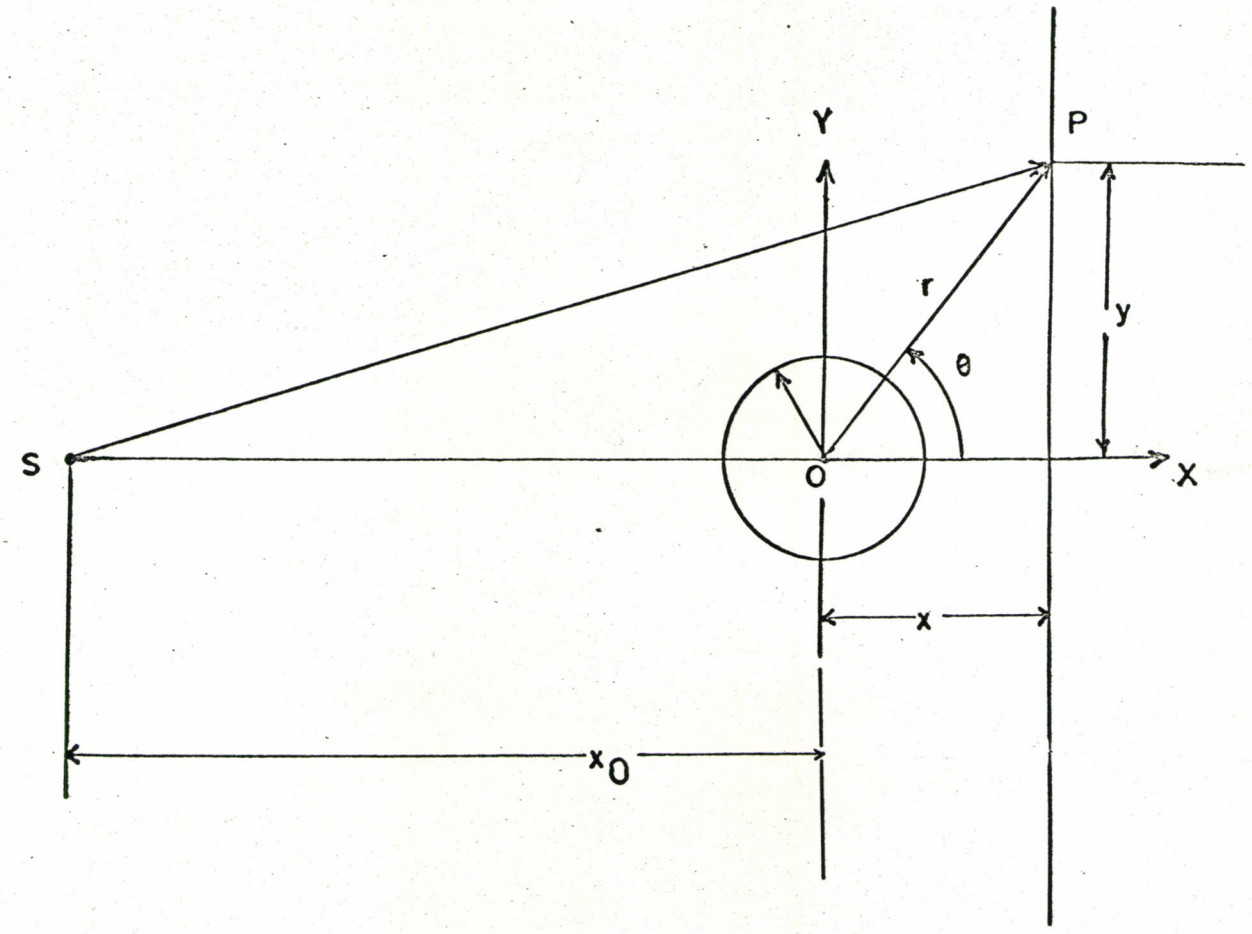

FIG. 2

$$(H_z)_{in} = H_o\, e^{ikx} \tag{2.2}$$

where,

$k = \frac{2\pi}{\lambda}$

$x = r \cos\theta$

H_o = field at $x = 0$.

Often it is convenient to expand this plane wave function in a Fourier series in θ, the coefficients being functions of r,

$$(H_z)_{in} = H_o\, e^{ikx} = H_o\, e^{ikr\cos\theta}$$

$$= H_o \sum_{m=0}^{\infty} C_m i^m J_m(kr) \cos m\theta \tag{2.3}$$

where,

$C_o = 1$ $\qquad$ $i = \sqrt{-1}$

$C_m = 2\ (m \neq 0)$ $\qquad$ $J_m(kr)$ are Bessel functions.

The wave effect at the point P scattered by the cylinder can be taken as a set of outgoing waves, given by,

$$(H_z)_{sc} = H_o \sum_{m=0}^{\infty} C_m A_m i^m H_m^{(1)}(kr) \cos m\theta \tag{2.4}$$

where,

$H_m^{(1)}(kr)$ is the Hankel function of the first kind (Weeks, 1964) and A_m is the amplitude of the scattered field which can be found by applying the boundary conditions. The resultant field at P is then

given by

$$(H_z)_{total} = (H_z)_{in} + (H_z)_{sc}$$

$$= H_o \sum_{m=0}^{\infty} C_m i^m \left[J_m (kr) + A_m H^{(1)} (kr) \right] \cos m\theta \tag{2.5}$$

where (see Appendix),

$$A_m = -\frac{\frac{1}{n} J_m (ka) J'_m (nka) - J_m (nka) J'_m (ka)}{\frac{1}{n} H_m^{(1)} (ka) J'_m (nka) - J_m (nka) H_m^{(1)'} (ka)} \tag{2.6}$$

Now, if we take the incident wave at P to be a cylindrical wave rather than a plane wave, then equation (2.3) can be written as

$$\frac{(H_z)_{total}}{H_o} = e^{i\phi_o} + \sum_{m=0}^{\infty} C_m i^m A_m H_m^{(1)} (kr) \cos m\theta \tag{2.7}$$

where,

$$\phi_o \simeq k \left[\left\{ (x + x_o)^2 + y^2 \right\}^{\frac{1}{2}} - x_o \right]$$

$$k = \frac{2\pi}{\lambda}$$

λ = free space wavelength

$$r = (x^2 + y^2)^{\frac{1}{2}}$$

$$n = \left(\frac{\mu_o \epsilon_1}{\mu_1 \epsilon_o} \right)^{\frac{1}{2}}$$

The electric component E_y of the field is related to the magnetic component H_z by,

$$\left(E_y\right)_{sc} = \frac{1}{i\omega\epsilon_o} \frac{\partial}{\partial x} \left[\left(H_z\right)_{sc}\right] \tag{2.8}$$

Therefore,

$$\left(\frac{E_y}{E_o}\right)_{total} = e^{i\phi_o} - \sum_{m=0}^{\infty} C_m i^{m-1} A_m F_m (r,\theta) \tag{2.9}$$

where (see Appendix),

$$F_m (r,\theta) = \cos\theta \cos m\theta \, H_m^{(1)'}(kr) + \frac{m \sin\theta \sin m\theta \, H_m^{(1)}(kr)}{kr} \tag{2.10}$$

The normalized intensities are proportional to the square of the normalized magnitude of the electric fields.

$$\frac{I}{I_o} \longrightarrow \left| \frac{E_y}{E_o} \right|^2 \tag{2.11}$$

This gives the normalized intensities in the diffraction patterns.

CHAPTER 3

EXPERIMENTAL ARRANGEMENTS

A. Standing Wave Patterns and Radiation Field Patterns

3-1 Microwave Generator

The microwave generator consists of a V-290 (VA-6314) klystron of Varian Associates which is capable of producing a minimum output of 50 mW to a maximum output of 110 mW. The klystron was pretuned to a frequency of 9.095 Gc (λ = 3.3 cm). The klystron was provided with a Hewlett-Packard Power Supply model No. 715 - A.

In order to keep the klystron temperature constant, a continuous flow of air was blown over the klystron. The power output of the klystron was fed into the X-Band RG - 52/U waveguide.

3-2 Microwave Components

To cut down the power level to a certain desired level, a Waveline Flap Attenuator, type No. 605, was used. The attenuator was adjustable from 0 to 20 db. To measure the frequency, a 20 db directional coupler was used to divert part of the microwave power to a Waveline frequency meter which had a quoted accuracy of 0.08%. The resonance in the wave meter was indicated by a dip of approximately 20% in the output.

A precision slotted line manufactured by Waveline Incorporated was used to measure the standing wave patterns. The precision slotted

line was the type No. 664 (8.4 Gc - 9.6 Gc) having an accurate and smooth control. A Sylvania 1N23C crystal was mounted in the probe carriage. A co-axial cable led to a microammeter having a range from 0 to 100 microamperes.

3-3 Waveguide Extension

The slotted line was connected to an extended piece of waveguide having a flange at one end only. The waveguide extension was bolted to the slotted line. The absence of a flange on the other end of the extended waveguide facilitated the study of radiation field patterns outside the waveguide. In the case of the standing wave patterns, this small piece of extension waveguide was replaced by an equivalent waveguide (same dimensions) having flanges on both ends. Therefore, the open end could be shorted if necessary.

3-4 Prisms

Two types of prisms (Fig. 3) were made for the purpose of studying the standing wave patterns inside the waveguide and the radiation field patterns in the transmitted wave. The dielectric prisms were made from a thermosetting plastic material called "Selectron 5026" (Pittsburg Plate Glass Company). Miniature prisms were constructed by cutting the material to the proper waveguide size and then smooth surfaces were achieved by polishing them with fine-grained sand paper. The dimensions of the prisms are shown in Fig. 3. Henceforth, the prism in Fig. 3(c) will be called Prism A and the prism in Fig. 3(d) will be called Prism B.

PRISMS AND THE FITTING OF THE PRISMS IN THE WAVEGUIDES

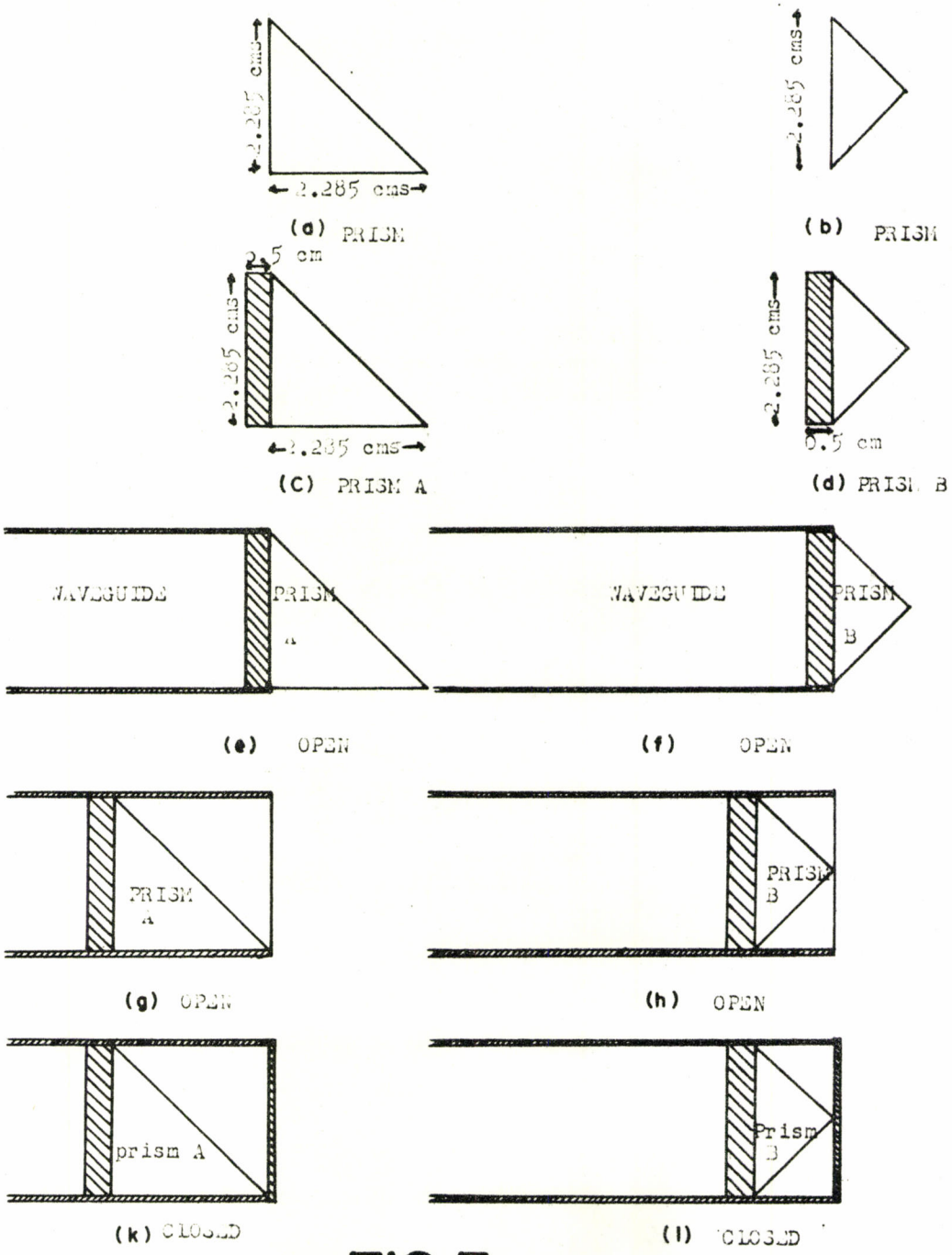

FIG·3

EXPERIMENTAL ARRANGEMENTS FOR THE INVESTIGATION OF GOOS-HAENCHEN SHIFT

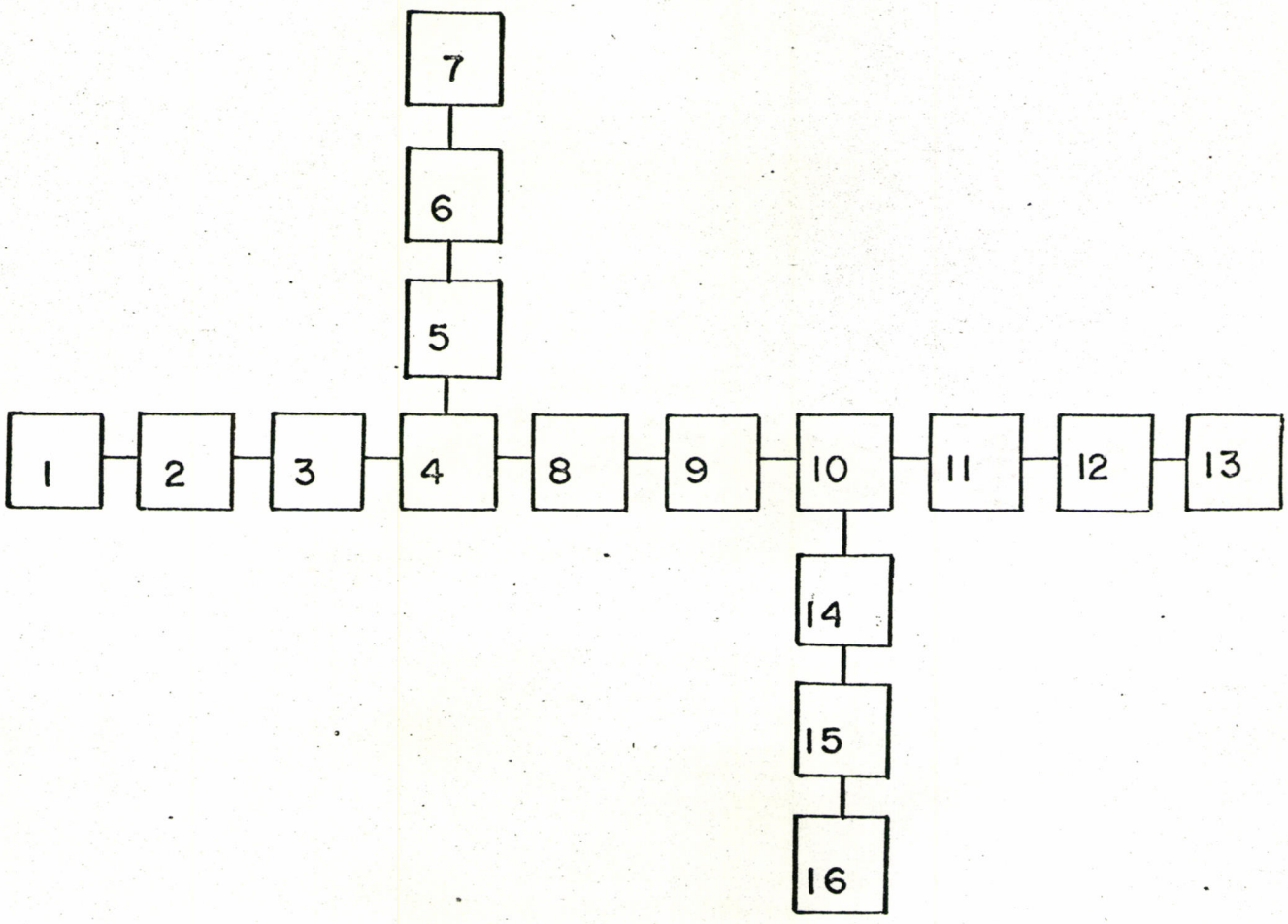

1. Klystron Power Supply
2. Klystron
3. Attenuator
4. Directional Coupler
5. Frequency Meter
6. Fixed Detector Mount
7. Micro Ammeter
8. Precision Slotted Line
9. E/H Tuner
10. H-Plane Tee
11, 14. Isolators
12, 15. Tunable Detector Mounts
13, 16. Micro Ammeters

FIG. 4

Another prism (Fig. 3(a)) which had the same dimensions as that of prism A, omitting the 0.5 cm extended strip, was also made. This prism was utilized in investigating the Goos-Haenchen shift.

B. Goos-Haenchen Shift

3-5 Additional Microwave Components

The experimental arrangements for the Goos-Haenchen shift has been shown in Fig. 4. An E/H tuner type No. 659 constructed by Waveline Incorporated was connected to the precision slotted line. The E/H tuner led to a Shunt Tee type No. 685 (Waveline Incorporated). Each of the arms (2) and (3) (Fig. 1(b)) of the Shunt Tee was provided with a Uniline ferrite isolator model R88-96 manufactured by Cascade Research.

As is shown in Fig. 4, block numbers 12 and 15 indicate the tunable detector mounts. The detector mounts, type No. 615, also had the same Sylvania cartridge detectors (1N23C).

C. Diffraction by Cylindrical Rods

3-6 Additional Microwave Components

In this experimental arrangement (Fig. 5), the microwave generator consisted of a different klystron (VA-242E) pretuned to a frequency of 9.375 Gc. The klystron power supply was an FXR Incorporated Model Z819B.

The component, block number 9, in Fig. 5 is a horn, constructed by C. E. Jordan (1960). This 10 cm aperture horn has a distance of 38.7 cm (i.e. from mouth to geometrical apex of opposite sides) in the H-plane

EXPERIMENTAL ARRANGEMENTS FOR THE MICROWAVE DIFFRACTION BY DIELECTRIC RODS

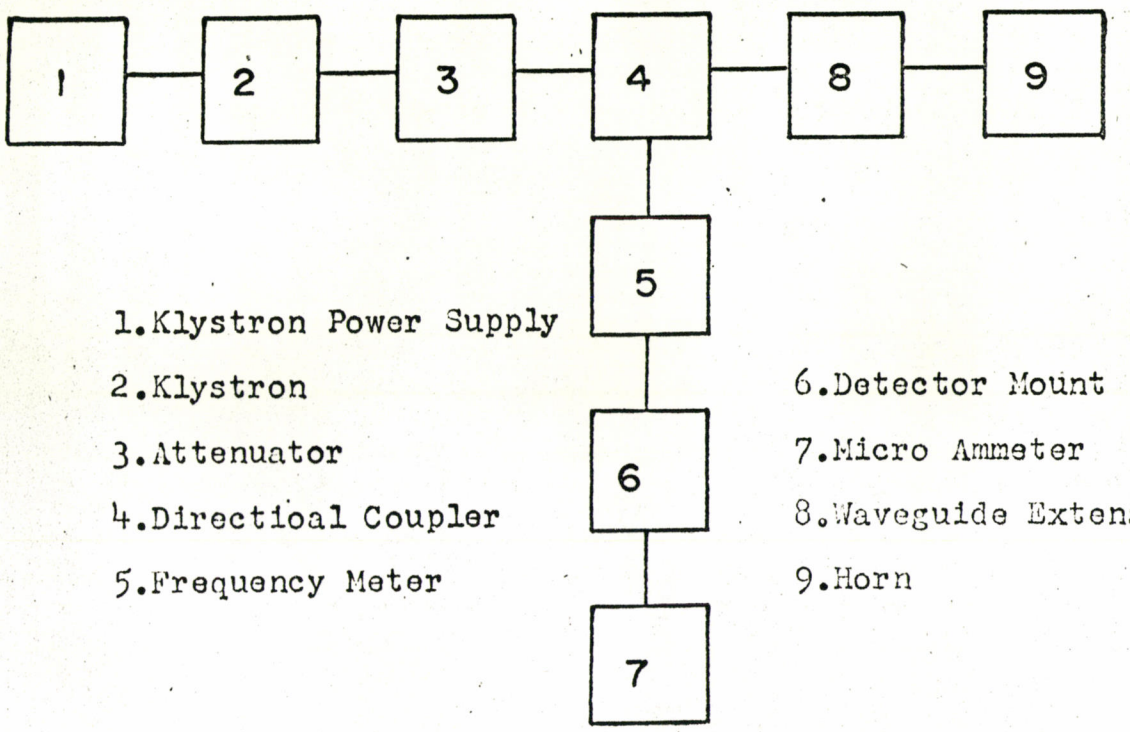

1.Klystron Power Supply
2.Klystron
3.Attenuator
4.Directioal Coupler
5.Frequency Meter

6.Detector Mount
7.Micro Ammeter
8.Waveguide Extension
9.Horn

lo.Detector Probe
11.Motor Assembly
12.Amplifier
13.Recorder

FIG.5

and 33.4 cm in the E-plane with flaring angles of 15° and 17° respectively. This horn provides a beam to approximate a cylindrical wave which is nearly a plane wave at a great distance.

The whole of the experimental set up was mounted on top of a strong metal frame at a height of 154 cm. The centre of the geometrical apex of the horn was at a height of 164 cm from the floor to minimize reflections from it.

3-7 Microwave Detector

A small 1 N 833 diode detector manufactured by Microwave Associates, 0.7 cm long and 0.25 cm in diameter, was used as a detector.

The leads of the diode were cut so that the total length of the diode was 1.6 cm ($\lambda/2$). Then the leads were soldered to those of the miniature co-axial cable taking care to use only a small drop of solder.

To hold the diode at a height of 164 cm, a glass rod support was made with 0.1 cm thick wall. The glass rod was tapered in three stages from an inside diameter of 0.7 cm to 0.35 cm. The 0.7 cm diameter part provided a strong base while the 0.35 cm (diameter) part just fitted the co-axial cable of the same diameter. The last part of the glass rod was bent through a right angle. The projected part after the bend was 153 cm above the floor and 44 cm long so that the diode could be at a distance 44 cm away from the rod and thereby reflections from the vertical part of the rod were minimized. This part could not be projected farther because the combined weight of the rod and cable would break the glass rod.

3-8 Track Assembly and Recorder

The probe was fixed onto a trolley which was moved upon an optical bench with the help of a reversible Bodine motor (1800 rpm and 1/25 h.p.). The speed of the motor was reduced by a factor of 50 with the help of a Boston transmission. All of the track was placed on a wooden box 8.5 cm high.

The recorder was a Universal Westronics Strip Chart Recorder Model No. S 11 A/U - 1/DV. 5M provided with an adjustable span. A chart paper feed speed of 4.0 inch/min was used.

3-9 Diffraction by Circular Rods

For the diffraction experiments, two dielectric rods of different diameters were used. One had a diameter of about 1 inch (a = 1.233 cm) and was 88.0 cm long while the other one had a diameter of about 1.5 inches (a = 1.916 cm) and was 145.0 cm long.

Two different rod holders were made to keep the cylinders perfectly vertical while taking the experimental observations. The dielectric rods were fastened to a heavy wooden base which was provided with levelling screws. The levelling screws were used to ensure that the axis of the rod was vertical.

3-10 Microwave Absorbers

Since the distance from the microwave horn to the rod was 5 meters, the beam spreads considerably and reflects from the walls, ceiling and floor of the room. This produces irregular standing wave pat-

terns in the room. To minimize these, microwave absorbers, 24 inch x 24 inch x 2 inch, obtained from the Sponge Rubber Products Company (Shelton, Connecticut) were used to cover the walls.

To cover the walls with these hair type absorbers, rectangular wooden frames were made and the microwave absorbers were then erected beside the walls. All of the ceiling could not be covered but the hanging beams in the ceiling were covered. The floor was also covered with the microwave absorbers.

CHAPTER 4

EXPERIMENTAL PROCEDURES

A. Standing Wave Patterns and Radiation Field Patterns

4-1 Stability of the Microwave Generator

The experimental set-up was followed as is shown in Fig. 6. An initial filament warm-up period of a couple of minutes was observed. The beam voltage was raised to the desired level to operate the klystron in a particular mode. Keeping the beam voltage constant, the reflector voltage was gradually varied until the maximum output for this mode was obtained. Setting the klystron to the condition of maximum power output makes the output insensitive to small changes in the reflector voltage and leads to a more constant output power. To achieve a stable frequency and a stable power output, the klystron was allowed to run for two hours before any experimental observation was made. During this time, the stability of the power output and the frequency were maintained.

When the frequency and the power were found to be sufficiently stable, the power transmitted down the waveguide was adjusted by the use of the flap attennator and was set for a suitable working power level. Then the probe plunger was gradually screwed in and a minimum possible penetration into the waveguide, consistent with a reasonable output signal from the probe, was maintained. This way

EXPERIMENTAL ARRANGEMENTS FOR THE STANDING WAVE PATTERNS AND THE RADIATION FIELD PATTERNS WITH THE OPEN WAVEGUIDE

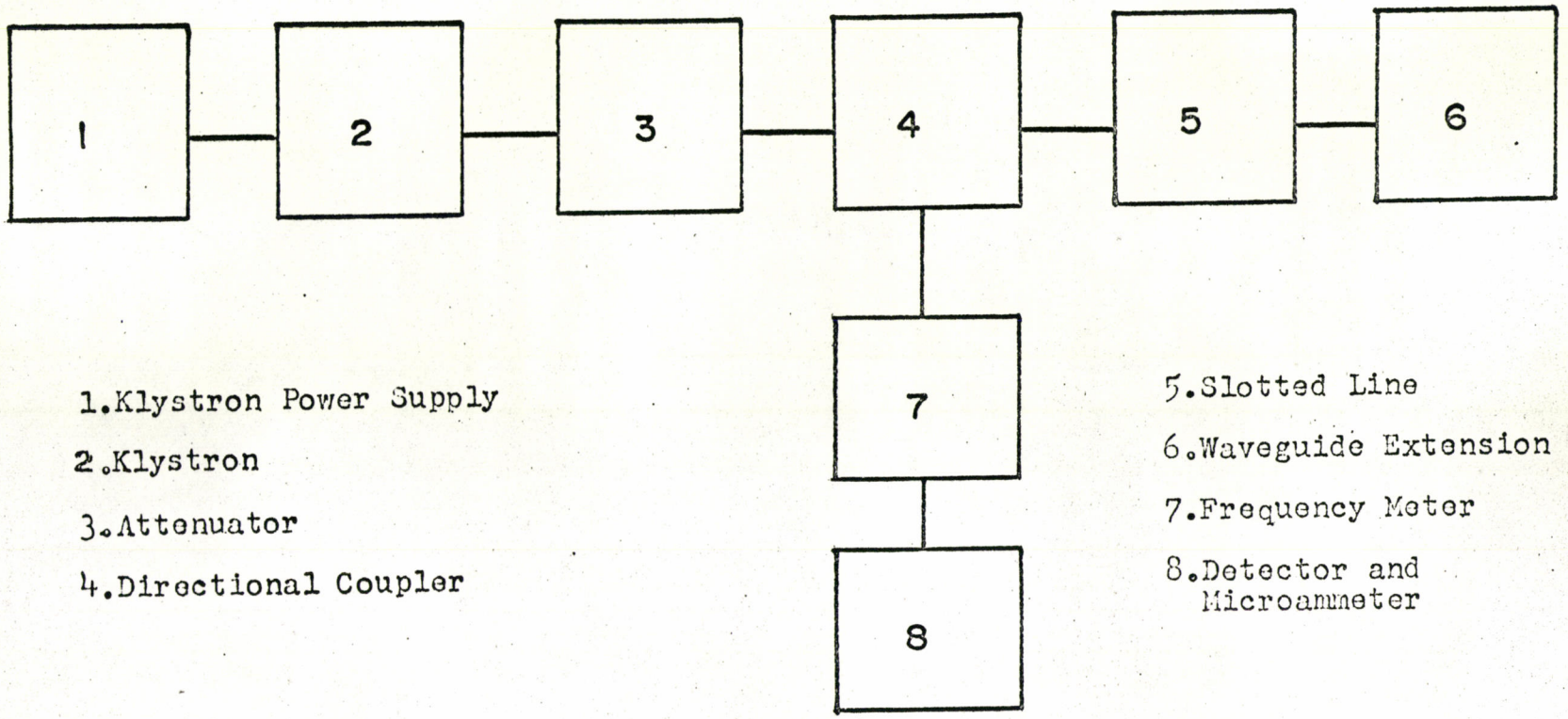

1. Klystron Power Supply
2. Klystron
3. Attenuator
4. Directional Coupler
5. Slotted Line
6. Waveguide Extension
7. Frequency Meter
8. Detector and Microammeter

FIG. 6

the reflection from the probe plunger could be minimized. The probe plunger was also provided with a tuning screw which was used to tune for a maximum probe signal output at a minimum penetration of the probe.

4-2 Standing Wave Patterns

The slotted line was connected with the extension waveguide with flanges on both ends. The end of the extension waveguide was short circuited with the help of a brass plate. Corresponding to the node at the short-circuited end, a node in the slotted line was selected as a reference node, and corresponding to the position of this reference node, the standing wave pattern was measured. This reference position was used in studying the standing wave patterns with the prisms, so that a comparative study could be made.

Observations of the probe detector current were made at intervals of 0.5 cm. The node positions of the standing wave pattern were noted carefully, since at this position, the change of the detector current is hardly noticeable. Therefore, a node position is hard to locate accurately. However, the best way of locating a node position was to take the average between two readings on either side of the node at a particular detector current, say, 1.0 micro-ampere. The readings, for the standing wave pattern were taken over a range of 8.0 cm.

Then prism A was introduced into the waveguide as shown in Fig. 3(e). Readings for the standing wave pattern were taken with prism A at the end. Next the prism A was pushed inside the waveguide

(Fig. 3(g)) and the readings for the standing wave pattern were repeated. Then the end of the waveguide was short circuited (Fig. 3(k)), and standing wave patterns were noted.

Similar observations were also made with prism B following similar steps shown in Fig. 3 (f, h, and 1).

4-3 Radiation Field Patterns

The extension waveguide for the standing wave pattern experiment was then replaced by the flangeless waveguide. The probe was placed at y = 0 (Fig. 7(a)) and the radiation field pattern for the E-plane of the waveguide was recorded by moving the probe along the X-axis (Fig. 7(a)). The signal was recorded at a speed 2 inch/min. The recorder adjusted such that the signal corresponding to the probe position at z = 0 (Fig. 7(a)), filled the whole chart span. Then the probe track was moved away from the waveguide end, (i.e., along Z-axis) runs were taken for z = 1,2,3... 7 cm.

Next the plane of polarization was rotated through a 90°-waveguide twist (Waveline Inc. Type No. 690). This waveguide twist was connected between the slotted line and extension waveguide. The detector probe was also turned through 90° so that the Electric Vector was parallel to the probe. Similar runs were taken for this geometry.

4-4 Radiation Fields with the Prisms

Next the twisted section of the waveguide was removed and the flangeless waveguide section was connected to the slotted line. The prism A was placed in the waveguide as shown in Fig. 3(e). The

COORDINATE AXES AND THE PRISMS

POINTING INSIDE THE WAVEGUIDES

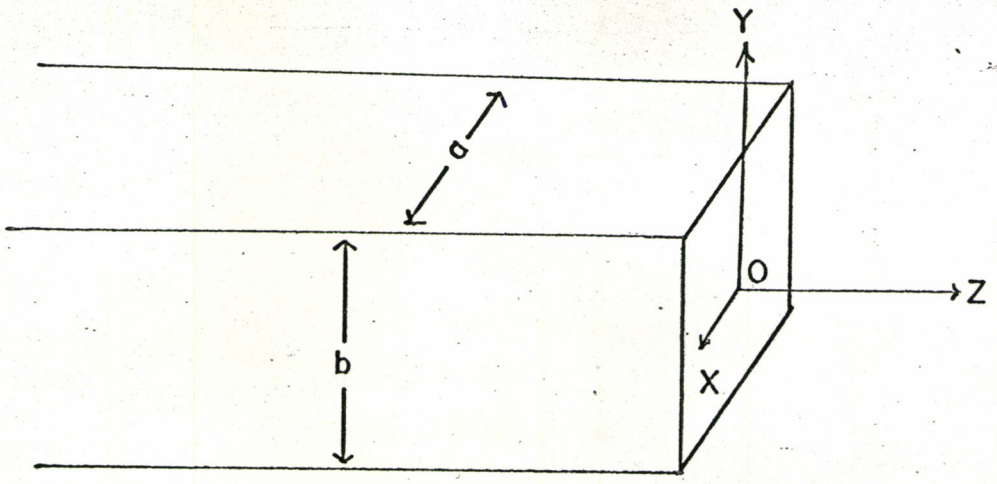

(a)

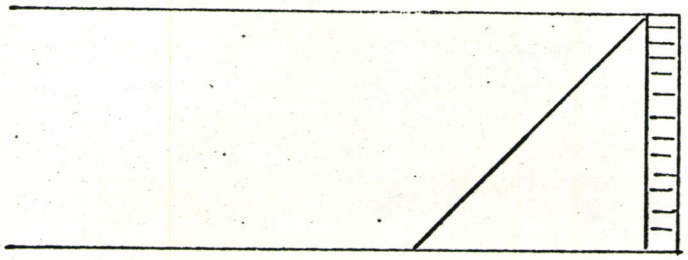

(b)

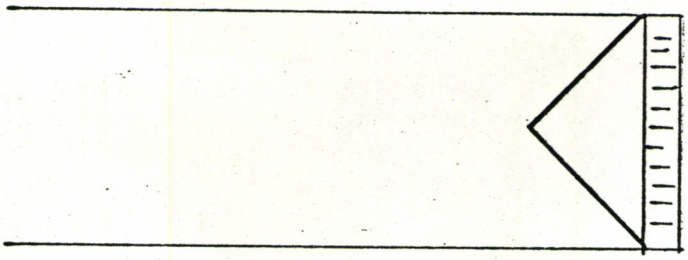

(c)

FIG·7

probe was placed at a distance z = 2.5 cm so that the probe could be run across the waveguide. One run was taken at z = 3.0 cm and then several runs were taken at intervals of 1.0 cm. Similar runs were taken with prism B (Fig. 3(f)).

Then the prism A was pushed into the waveguide as shown in Fig. 7 (b and c). Similar runs were taken with prism A and prisms B, starting from z = 2.5 cm.

B. Goos-Haenchen Shift

4-5 Experimental Procedure

For the investigation of the Goos-Haenchen shift, the prism shown in Fig. 3(a), was used. The experimental set-up was followed as shown in Fig. 5. After checking the stability of the power and frequency, the tuning of the E/H tuner and the detector mount were made. The prism (Fig. 3(a)) was inserted into the arm (1) of the Shunt Tee as shown in Fig. 1(b). The prism was pushed towards the shunt junction at intervals of 0.5 cm and the detector currents were measured in arms (2) and (3). This was repeated until the prism passed the junction by a few centimeters.

C. Diffraction by Cylindrical Rods

4-6 Alignment of the Horn

The level of the waveguide component was adjusted so that the central axis of the horn was parallel to the floor. A thin pencil mark was drawn on the centre of the surface of the horn and parallel to which a thin thread was run all the way to the end of the

room. At the end of the thread, a small piece of paper was placed, which was located by a telescope attached to the waveguide and then the thread and the pencil mark on the horn were made parallel by tilting the horn. This way the X-axis was fixed and was made parallel to the floor.

4-7 Placing of the Rod at the Centre

Although the experimental situations seem to be very simple, the complete alignments of the experiment is very difficult. This alignment has to be done very carefully to ensure the accuracy of the results. To locate the central apex of the horn, the end of the horn was projected on the floor and was marked. In this way, the source S was located 33.4 cm behind this mark. Then the whole of the thread was projected on the floor and distances from the apex of the horn were measured off on it.

Two pencil marks divided the rod mount into four quadrants and then the centre of these two crossing lines on the base of the rod mount, was placed at OS = 5 meters.

A white piece of paper as long as the diameter of the rod was divided into four equal parts by marking with a pencil and then this marked paper was wrapped around the rod marking the pencil marks on the floor, and on the paper parallel. Since the pencil marks on the floor were made parallel along the X and Y axes already, the alignments of the wrapped paper pencil marks with those of the floor made the diameters of the rod also parallel to the X and Y axes. In this way, the X and Y axes were set at the centre of the rod. To

set the Z-axis of the rod, the rod was adjusted to be vertical with the help of a spirit level. Therefore, the axes of the co-ordinate system (Fig. 2) were set completely.

4-8 Probe Alignment

The track assembly was placed behind the rod and the optical bench was set perpendicular to the X-axis. The holder was rotated until the microwave diode was parallel to the Y-axis and then the diode was rotated until it became (almost) perpendicular to the Z-axis but parallel to the X-axis.

4-9 Procedure for Taking the Runs

(a) At x = 0 (along Y-axis):

The track was placed such that the probe was at x = 0. A run was taken for the incident field without any rod. The run was taken over a distance of 40 cm along the Y-axis, 20 cm on either side of y = 0.

The rod was then placed at the origin so that both the rod and the probe were at x = 0; the probe can record the diffraction field only on one side in a single run. To record the field on the other side, the probe holder was pulled back a little and the trolley was moved to the other side without moving the track. To get a symmetric field on either side of the rod, the important considerations are: (i) the rod is perfectly vertical; (ii) the probe is on a plane parallel to the Y-axis. The latter condition was satisfied by checking that the probe leads were just on the pencil marks set on the paper wrapped around the rod.

Runs were taken by moving the probe from y = 20 cm to y = (a + 0.5 cm), a = 1.916 cm or 1.233 cm. The probe was stopped at 0.5 cm before it touched the surface of the rod to ensure that the probe plane would not change. In this way, the field on one side of the rod was recorded.

To record the field on the other side of the rod, the probe was placed at y = -(a + 0.5) cm and then allowed to run out to y = -20 cm. The motor direction was changed and the above procedure was repeated. An average was taken to get the reading for the field at x = 0.

(b) At x = 1.6 cm, 3.2 cm, 4.8 cm, 6.4 cm and 8.0 cm:

To make runs at the above x-values (multiples of $\lambda/2$), the rod was moved away from the probe towards the source. It was easier to move the rod than the track, since the track was difficult to align parallel to the Y-axis.

To move the rod accurately, a meter stick was placed touching the side of the rod mount. Two heavy weights were placed at both ends of the meter stick so that the meter stick did not move. The rod mount was slid along the meter stick where the x-positions were read. At five different values of x, the diffraction patterns were recorded.

For the small rod (a = 1.233 cm), an additional run was taken at x = 1.3 cm. For the larger rod (a = 1.916 cm) another run was taken at x = 2.2 cm. These two particular x-values corresponded to the cases where the probe almost touched the surface of the rod at the X-axis. Runs corresponding to other values of x (multiples of

$\lambda/2$), were the same for both the rods.

(c) At y = 0 (along X-axis):

The probe holder was then rotated through 90°. The track was placed parallel to the X-axis. A run was taken for the incident field. Then the rod was placed at the centre (OS = 5 meters). Runs were taken for both the rods along the X-axis away from the source. Again, the probe was not allowed to touch the rod for the same reason, as noted above.

CHAPTER 5

RESULTS AND DISCUSSIONS

5-1 Standing wave patterns with Prism A

The results for the standing wave patterns with prism A have been shown in Fig. 8. Increasing probe position represents an increasing distance from the prism. The standing wave pattern for the short circuited case without any prism, has been shown with a thick continuous curve. Corresponding to this curve, a comparative study of the standing wave patterns were made. The single dotted curve shows the short circuited case with prism A (Fig. 3 (k)). Comparing this with the short circuited case, we see that there is a 10% decrease in the intensity and there is a relative phase difference of about 20°. Since the wave travels at a different velocity in the dielectric prism region, the whole of the standing wave pattern is shifted through a 20° phase angle.

The double dotted line shows the standing wave pattern with Prism A with the end of the guide open (Fig. 3(e)). There is a 53% reduction of intensity and a phase difference of 20°. This shows that a part of the incident wave is transmitted to the free space, while the other part of the wave reflected back produces standing waves. The amplitude at the node in this case is zero again showing that there is a transmission of energy into the free space beyond the

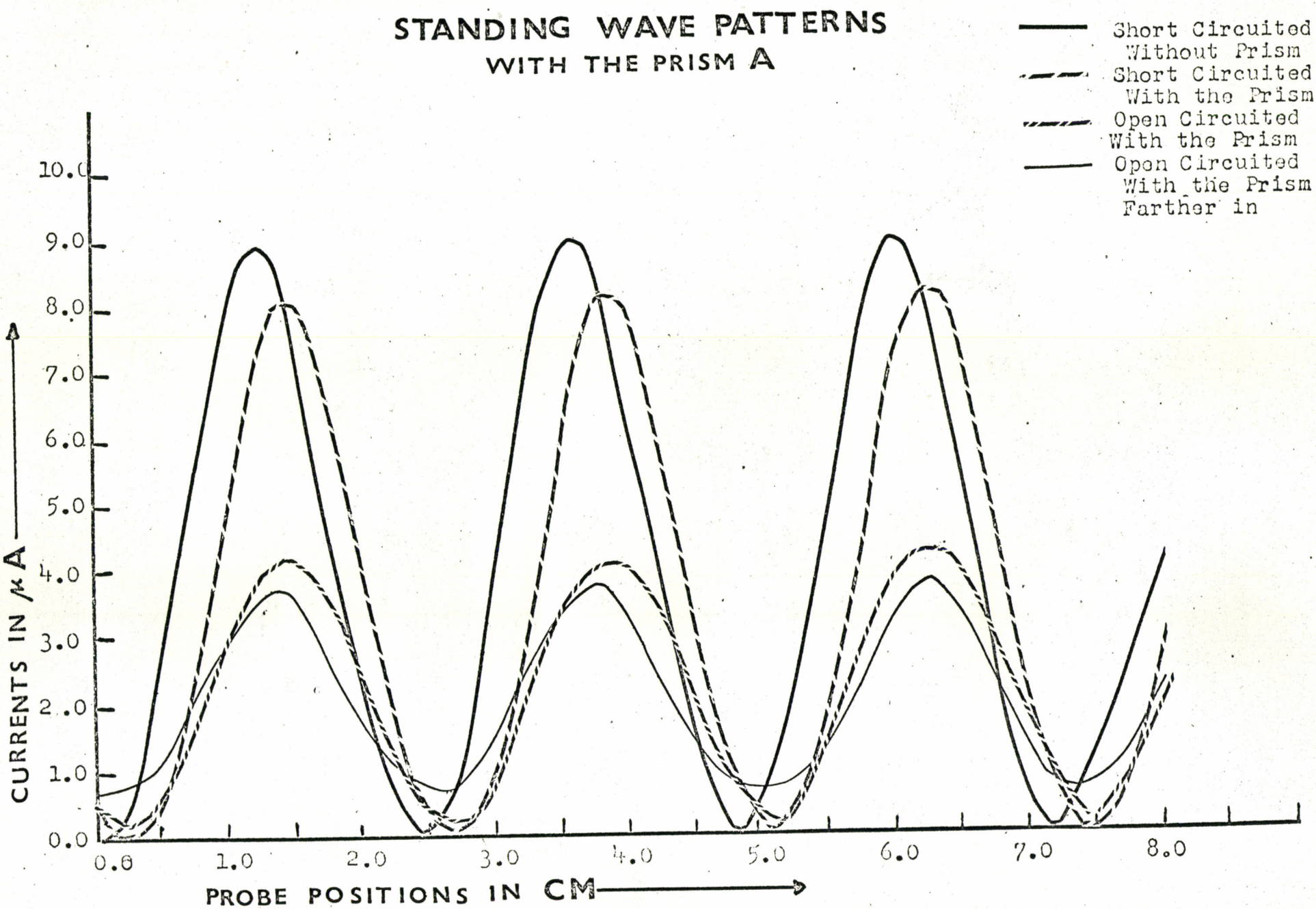
STANDING WAVE PATTERNS
WITH THE PRISM A
Short Circuited Without Prism
Short Circuited With the Prism
Open Circuited With the Prism
Open Circuited With the Prism Farther in
CURRENTS IN μA
10.0
9.0
8.0
7.0
6.0
5.0
4.0
3.0
2.0
1.0
0.0
0.0
1.0
2.0
3.0
4.0
5.0
6.0
7.0
8.0
PROBE POSITIONS IN CM

FIG·8

the waveguide. The light, continuous line is for the case shown in Fig. 3(g). There is a 58% reduction of intensity.

5-2 Standing Wave Patterns with Prism B

The standing wave patterns with prism B have been shown in Fig. 9. Again a comparative study is made with the short circuited case without any prism (the continuous heavy curve). The single dotted curve indicates the results for the case shown in Fig. 3(l). It shows that there is a phase change of about 176° and a 20% decrease in the intensity. If we compare this with that of Prism A, we see that Prism B introduces a greater change in the standing wave pattern than Prism A.

Again the double dotted line is for the case shown in Fig. 3(f). This shows that the whole of the standing wave pattern has shifted to the left by -26° and there is a 39% reduction of the intensity. That is, there is less reduction of the intensity compared to that of prism A (53%). This shows that prism B transmitted less energy into the free space and reflected wave energy back into the waveguide.

However, the thin continuous line shows apparently a contradition to the above argument. In this case, since prism B (Fig. 3(h)) is inside the guide, the brass waveguide walls had more influence on the distribution of the field than that of the prism.

5-3 Radiation Field Patterns with the Open Waveguide

Radiation field patterns (without prism) from an open waveguide are shown in Fig. 10. The central vertical line shows the arbitrary intensity scale while the left and right vertical lines show the distances along the Z-axis (Fig. 7(a)). The bottom horizontal line shows the distances along the x-axis. Since the

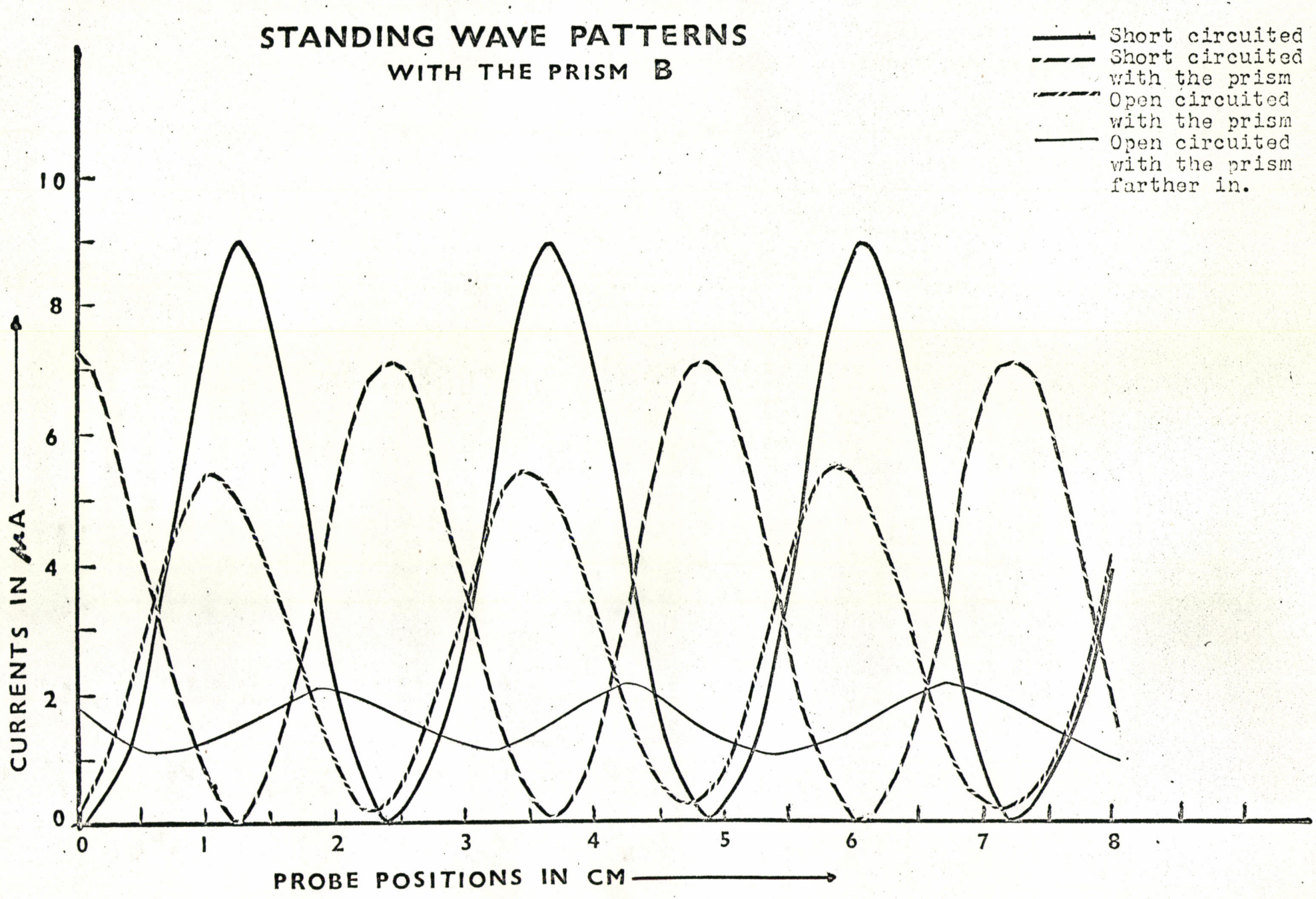
STANDING WAVE PATTERNS
WITH THE PRISM B
Short circuited
Short circuited with the prism
Open circuited with the prism
Open circuited with the prism farther in.
CURRENTS IN μA
10
8
6
4
2
0
0
1
2
3
4
5
6
7
8
PROBE POSITIONS IN CM

FIG·9

fields were found to be symmetric, only the right halves of the intensity patterns are shown. Fig. 10(a) shows the patterns in the E-plane of the waveguide, while Fig. 10(b) showsthem for the H-plane.

The intensity corresponding to z = 0 shows a very sharp peak and then falls off very rapidly. As z increases, the intensity decreases very rapidly, and shows a small variation along the X-axis for large z. For z = 0, in Fig. 10(b), the intensity pattern shows a hump which may be due to the asymmetry of the probe.

5-4 Radiation Fields with Prism A and Prism B Pointing Inside the Waveguide

The radiation field patterns for prism A and prism B pointing inside the waveguide (Fig. 7, b and c respectively), are shown in Fig. 11. Three sets of radiation field patterns, without prism, with prism A, and with prism B, are shown on the same scale so that a comparative study could be made. The bottom horizontal axes are the X-axes (Fig. 7(a)) of the waveguide. On the extreme left, the intensities are shown, while at the extreme right the distances along the Z-axis are shown. The positions of the prisms are shown at the bottom of the two left graphs.

If we compare the intensity patterns for the three curves, for a particular z-value, say, z = 2.5 cm, we see that the intensity has dropped by 20% with prism A and by 40% with prism B. This is also true for any other z-value showing that the whole of the intensity pattern has been reduced, when the prism is introduced as shown in Fig. 11. This reducing effect of the prisms suggests that the prisms are reflecting energy back into the waveguide. In this respect,

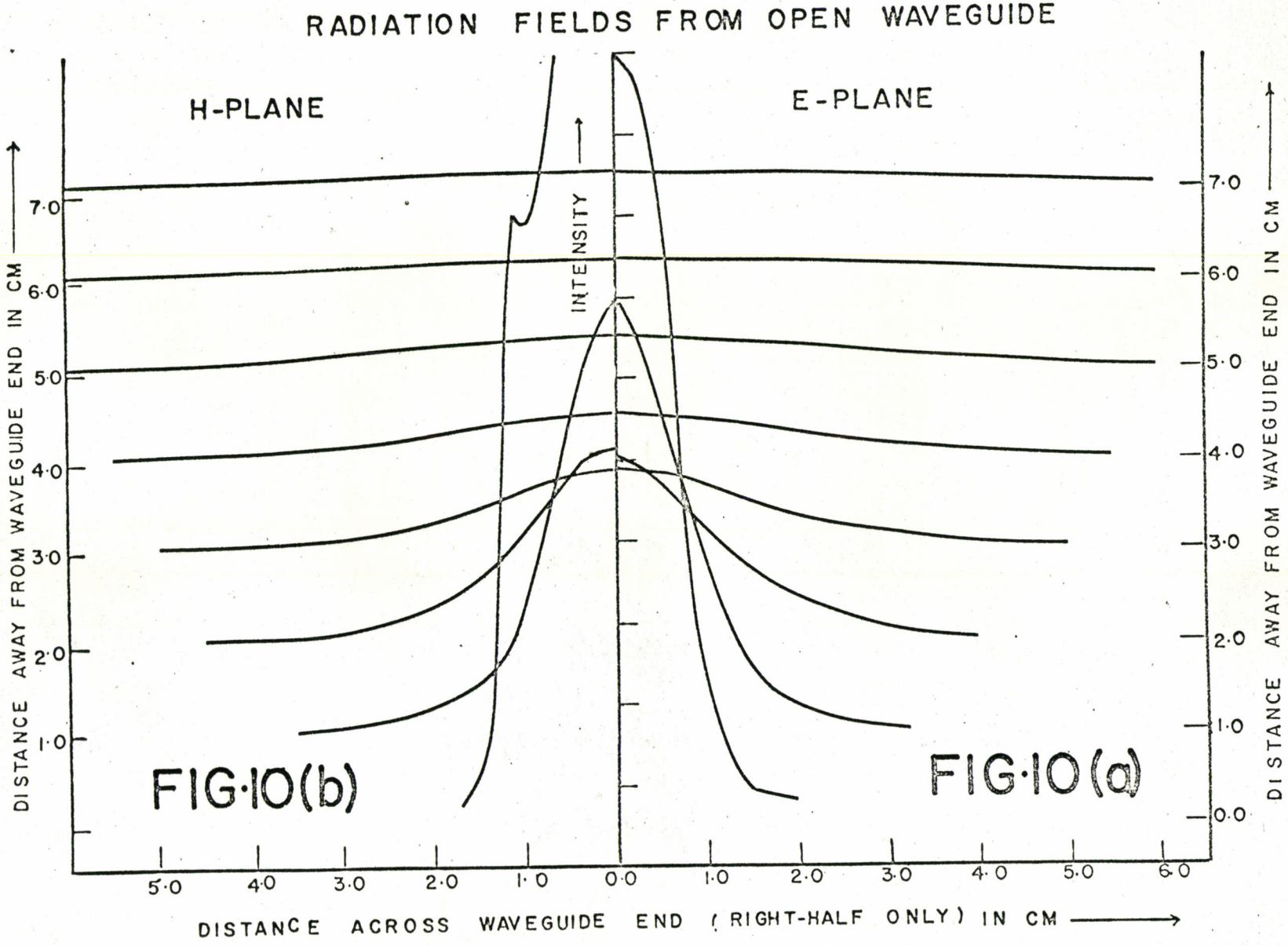
RADIATION FIELDS FROM OPEN WAVEGUIDE
H-PLANE
E-PLANE
INTENSITY
DISTANCE AWAY FROM WAVEGUIDE END IN CM
7·0
6·0
5·0
4·0
3·0
2·0
1·0
0·0
5·0
4·0
3·0
2·0
1·0
0·0
1·0
2·0
3·0
4·0
5·0
6·0
DISTANCE ACROSS WAVEGUIDE END (RIGHT-HALF ONLY) IN CM
FIG·10(b)
FIG·10(a)

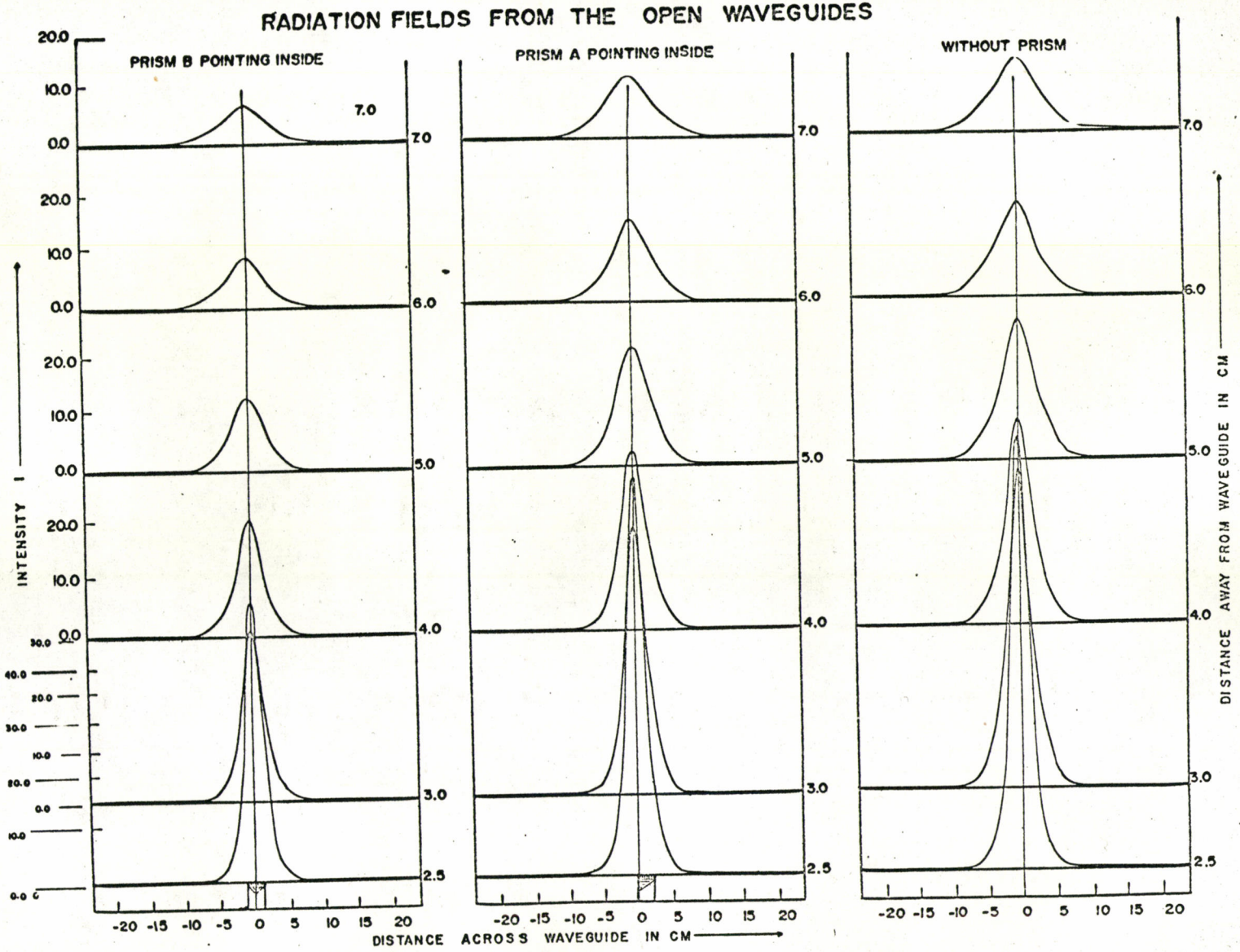
RADIATION FIELDS FROM THE OPEN WAVEGUIDES
PRISM B POINTING INSIDE
PRISM A POINTING INSIDE
WITHOUT PRISM
INTENSITY I
DISTANCE AWAY FROM WAVEGUIDE IN CM
DISTANCE ACROSS WAVEGUIDE IN CM
7.0
6.0
5.0
4.0
3.0
2.5
20.0
10.0
0.0
-20 -15 -10 -5 0 5 10 15 20

FIG. 11

prism B is a better reflector than prism A.

Another point that has been noted is the distribution of the intensity peaks. With prism B, the central peaks are symmetric about the central projected axis of the waveguide, and hence about the central tip of prism B. With prism A, the central peaks are also centred around the tip of prism A, but not about the projected waveguide axis. The whole of the intensity pattern for prism A has been shifted to the left.

5-5 Radiation Fields with Prism A and Prism B pointing Outside

The radiation fields are shown in Fig. 12. The prisms are also shown in the figures. Prism A shows a 25% increase in the intensity while prism B shows 17% increase, relative to the open guide case. This increase in intensity suggests that the prisms concentrate the fields at the tip of the prisms protruding from the guide.

The walls of the dielectric prism act as boundary walls guiding the power towards the tip. In this regard, prism A is more effective than prism B. The positions of the central peaks are similar to those of Fig. 11.

5-6 Goos-Haenchen Shift

The results of the investigation of G-H shift have been shown in Fig. 13. The continuous curve shows currents in arm (3) and the dotted line shows currents in arm (2), with respect to the prism position x (Fig. 1(b)). For the prism position x = 3.3 cm, the shunt arm current reaches a maximum and at the same time, the arm (2) current drops to a minimum. Fig. 13 shows the prism position corresponding

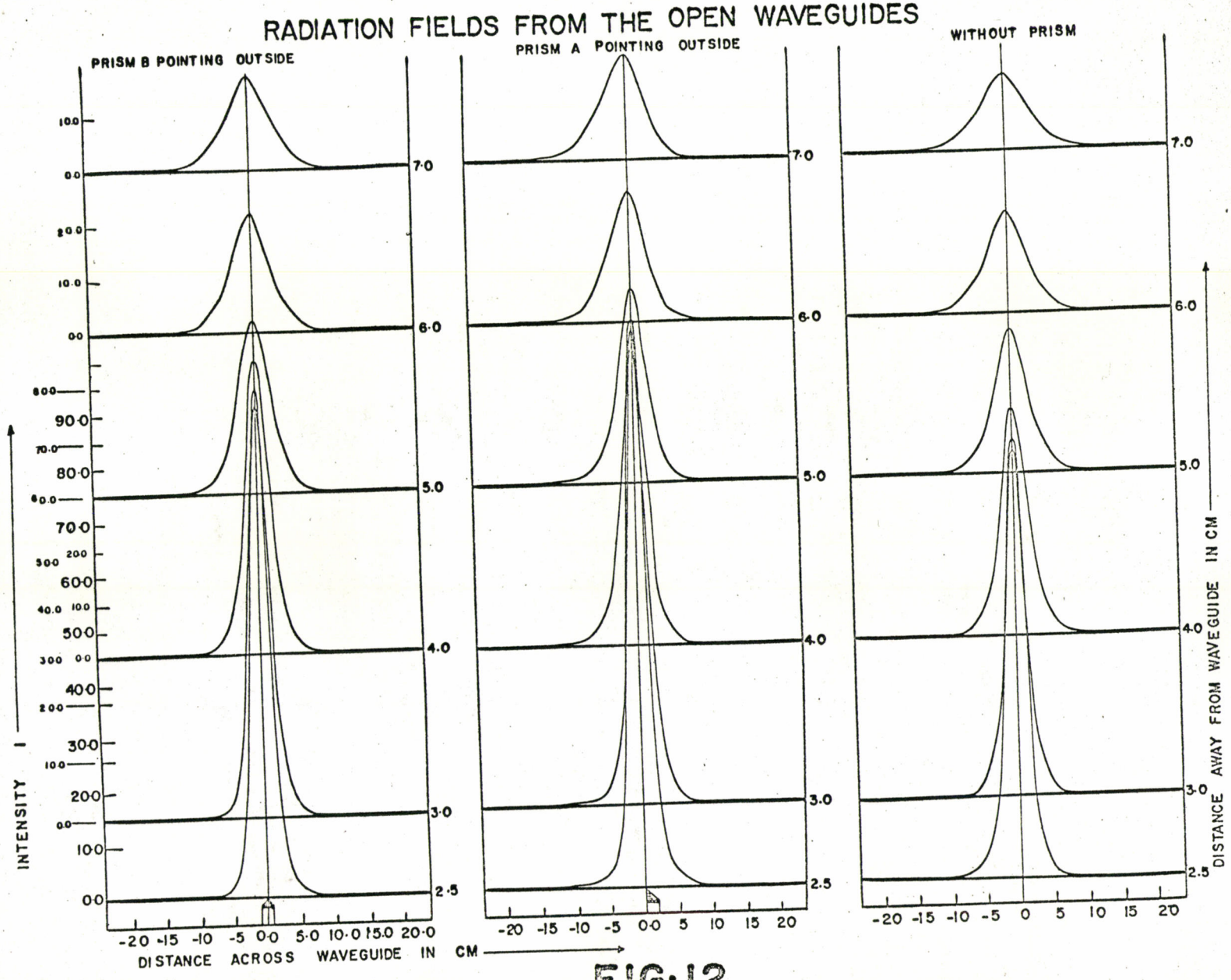
RADIATION FIELDS FROM THE OPEN WAVEGUIDES
PRISM B POINTING OUTSIDE
PRISM A POINTING OUTSIDE
WITHOUT PRISM
INTENSITY I
DISTANCE ACROSS WAVEGUIDE IN CM
DISTANCE AWAY FROM WAVEGUIDE IN CM
7·0
6·0
5·0
4·0
3·0
2·5
-20 -15 -10 -5 0·0 5·0 10·0 15·0 20·0
-20 -15 -10 -5 0·0 5 10 15 20
-20 -15 -10 -5 0 5 10 15 20

FIG·12

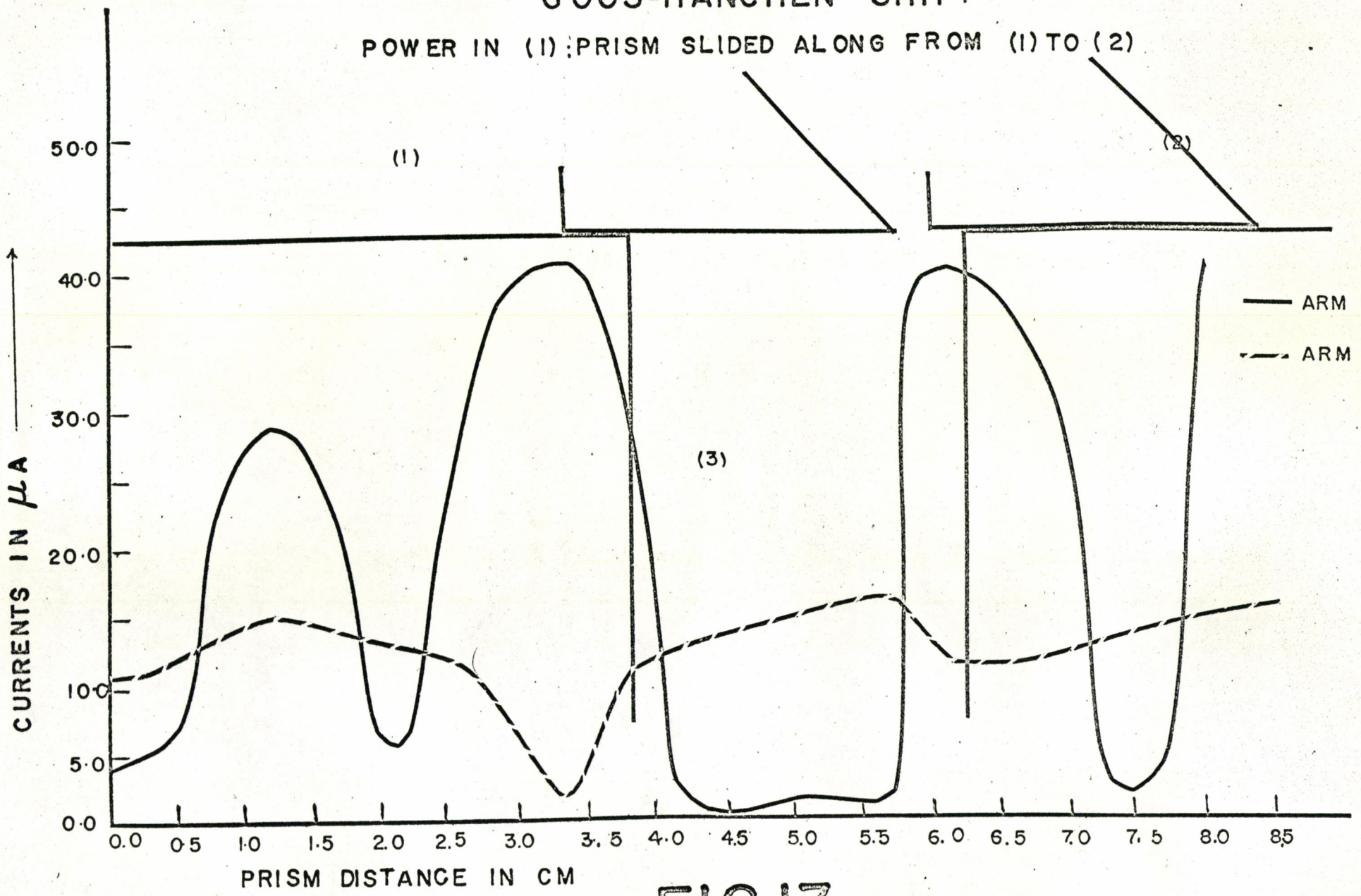
GOOS-HÄNCHEN SHIFT
POWER IN (1) : PRISM SLIDED ALONG FROM (1) TO (2)
(1)
(2)
(3)
50·0
40·0
30·0
20·0
10·0
5·0
0·0
CURRENTS IN μA
ARM (3
ARM (2
0.0 0·5 1·0 1·5 2.0 2.5 3.0 3.5 4·0 4.5 5.0 5.5 6.0 6.5 7.0 7.5 8.0 8.5
PRISM DISTANCE IN CM

FIG·13

to the maximum shunt current. From calculations of the G-H shift, the reflected beam from the prism is expected at x = 4.5 cm, but the shunt current is measured at the centre of the shunt arm, which is at a distance x = 5.1 cm. The difference between these two readings gives d = 0.6 cm. However, a calculation from equation (2.1) shows d = 1.02 cm for a 45^{o} angle of incidence. Therefore, the results do not agree.

Another maximum was found for the prism position x = 6 cm. This maximum shunt current had almost the same magnitude as that at x = 3.3 cm. The current in arm (2) has also dropped but not the same amount as before.

These results suggest that the current maxima obtained in arm (3) are not due to the G-H shift. As has been explained in other prism experiments, the prism at x = 3.3 cm also is concentrating the power in its tip and throwing more power in arm (3). The prism at x = 6 cm shows that the prism reflects the incident wave so that the reflected wave enters arm (3) and gives a maximum.

5-7 Diffraction by Cylindrical Rods, Incident Field at x = 0 (along Y-axis)

The incident field along the Y-axis has been shown in Fig. 14. The fields on both sides of the origin are shown. Since the reflections from sidewalls etc. could not be avoided completely, an irregular standing wave pattern shows up in the incident field. Fig. 14 shows the best incident wave that was recorded. The field on either side of the origin is not very symmetric, especially around y = -15 cm. However,

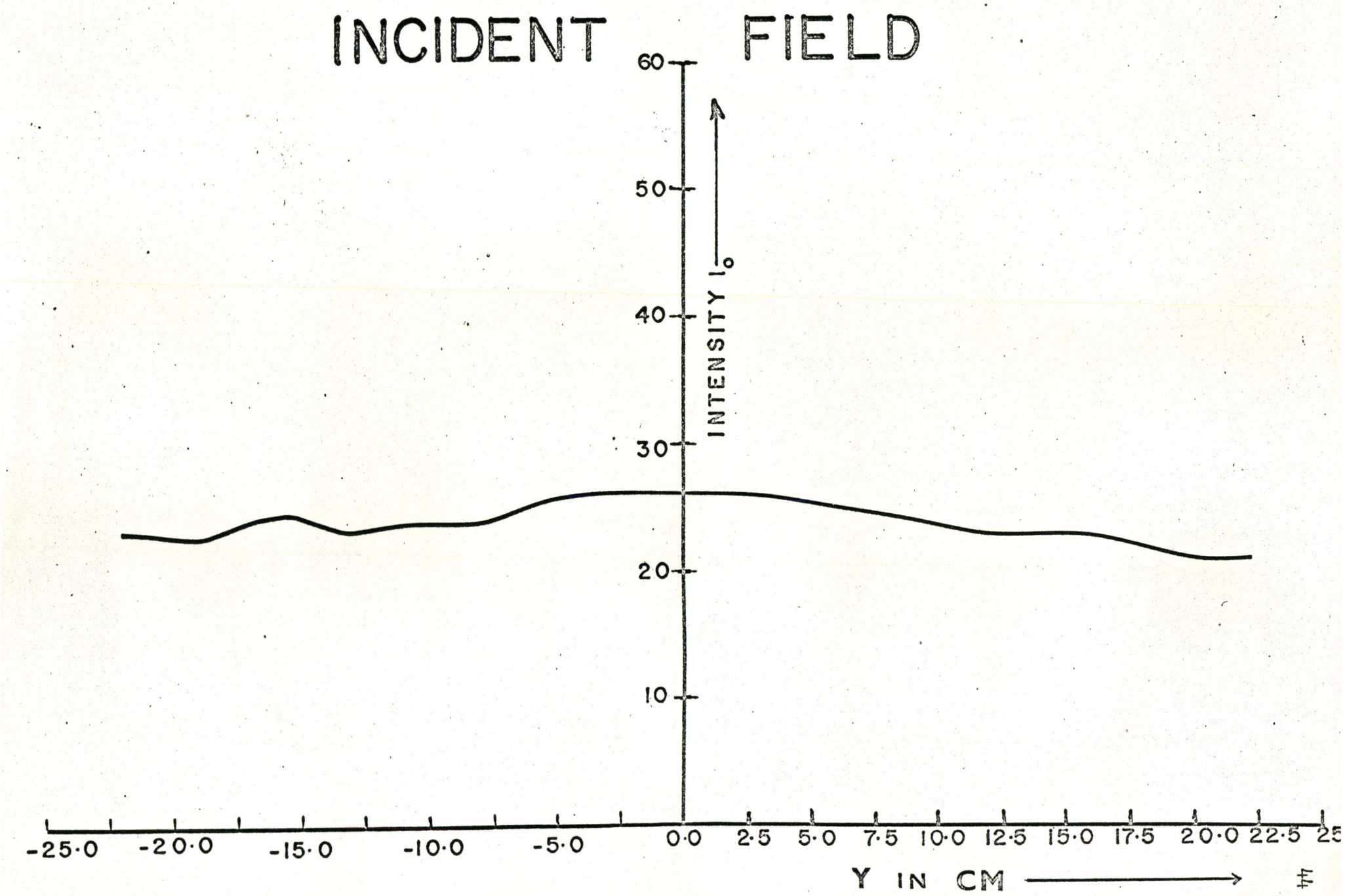
INCIDENT FIELD
60
50
40
30
20
10
INTENSITY I_o
-25·0
-20·0
-15·0
-10·0
-5·0
0·0
2·5
5·0
7·5
10·0
12·5
15·0
17·5
20·0
22·5
Y IN CM

FIG. 14

this would not affect the result much since the total field is normalized.

5-8 Normalized Diffraction Patterns for 1.5 inch and 1.0 inch Rods

Fig. 15 and Fig. 16 show the normalized diffraction patterns for the 1.5 inch and 1.0 inch lucite rods, respectively. The central vertical line shows the normalized intensities while the two other solid vertical lines show the surface boundaries of the rods. The calculated and experimental results are shown in the figures.

There is a discrepancy in phases as well as in the amplitudes which can be seen by comparing the experimental and calculated results. The reasons for the discrepancies may be due to one or more of the following causes. At x = 0, there are Ex and Ey components of the electric vector scattered from the cylindrical rod. A slight misalignment might cause the diode to pick up less of the Ey-component. It has also been noticed that the diode leads were not exactly in a line. Therefore, each of the diode leads would pick up different fields. Again, maybe the diode length was not exactly a half wavelength dipole. Similar variations between experiment and theory are seen for both diameter rods.

5-9 Unnormalized Diffraction Patterns for 1.5 inch and 1.0 inch Rods

The unnormalized diffraction patterns for both rods have been shown in Fig. 17 and Fig. 18. The unnormalized diffraction patterns show the relative changes in the pattern and a comparative study could be made very easily. The diffraction patterns show

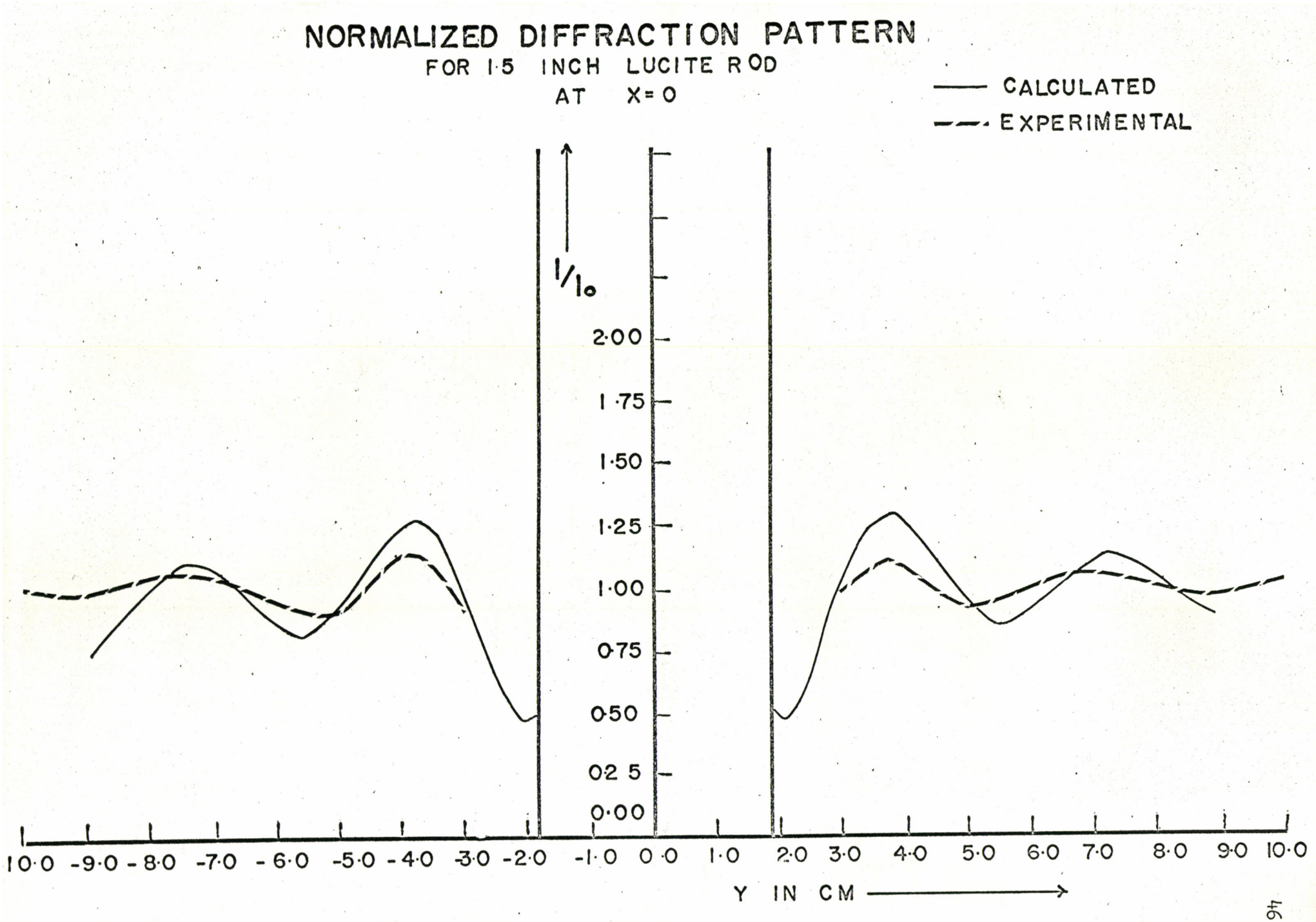
NORMALIZED DIFFRACTION PATTERN
FOR 1·5 INCH LUCITE ROD
AT X=0
CALCULATED
EXPERIMENTAL
I/Io
2·00
1·75
1·50
1·25
1·00
0·75
0·50
0·25
0·00
10·0 -9·0 -8·0 -7·0 -6·0 -5·0 -4·0 -3·0 -2·0 -1·0 0·0 1·0 2·0 3·0 4·0 5·0 6·0 7·0 8·0 9·0 10·0
Y IN CM

FIG·15

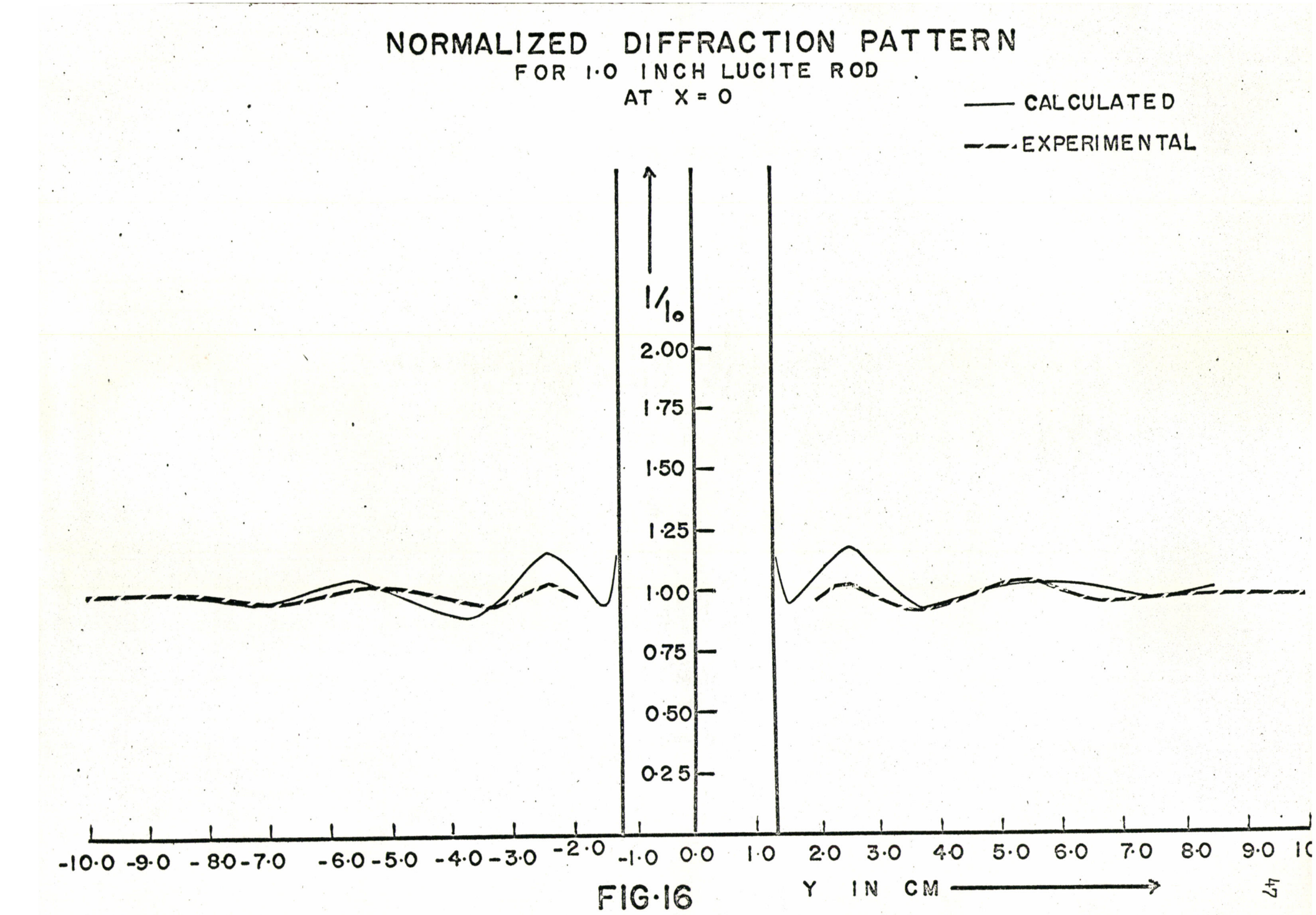
NORMALIZED DIFFRACTION PATTERN
FOR 1·0 INCH LUCITE ROD
AT X = 0
CALCULATED
EXPERIMENTAL
I/I₀
2·00
1·75
1·50
1·25
1·00
0·75
0·50
0·25
-10·0 -9·0 -8·0 -7·0 -6·0 -5·0 -4·0 -3·0 -2·0 -1·0 0·0 1·0 2·0 3·0 4·0 5·0 6·0 7·0 8·0 9·0
Y IN CM

FIG·16

pronounced maxima and minima behind the rods. In the close vicinity of the rod, the central maxima are much higher than the other maxima. The 1.5 inch rod shows a hump at y = 4.8 cms. in the x = 3.2 cm pattern. This grows larger and the central peak gets smaller with increasing x. For the 1.0 inch rod, this hump does not show up. However, it also shows the central peak decreasing and the other peak increases with increasing x as in the case of the 1.5 inch rod.

The incident field at the first surface of the rod can be divided into two parts, a transmitted part and a scattered part. A similar division can also be at the second surface. However, only the transmitted wave is of interest. The superposition of the transmitted and the scattered field gives the diffraction patterns. The prominent features have been explained in part by geometrical optics by Subbarao and McLay (1956).

5-10 Incident Field Along X-axis

The fields along the X-axis have also been studied. Fig. 19 shows the shape of the incident field. The heavy black curve shows the actual incident field behind the rod but along the X-axis of propagation of the beam. This actual field shows an irregular standing wave pattern. This shows that there were lots of reflections from the walls. This could not be avoided in spite of the double layer shielding on the wall. A heavy dotted line shows the average of the incident field. For normalization purposes, the average field was used.

UNNORMALIZED DIFFRACTION PATTERNS

FOR 1·5 INCH LUCITE ROD

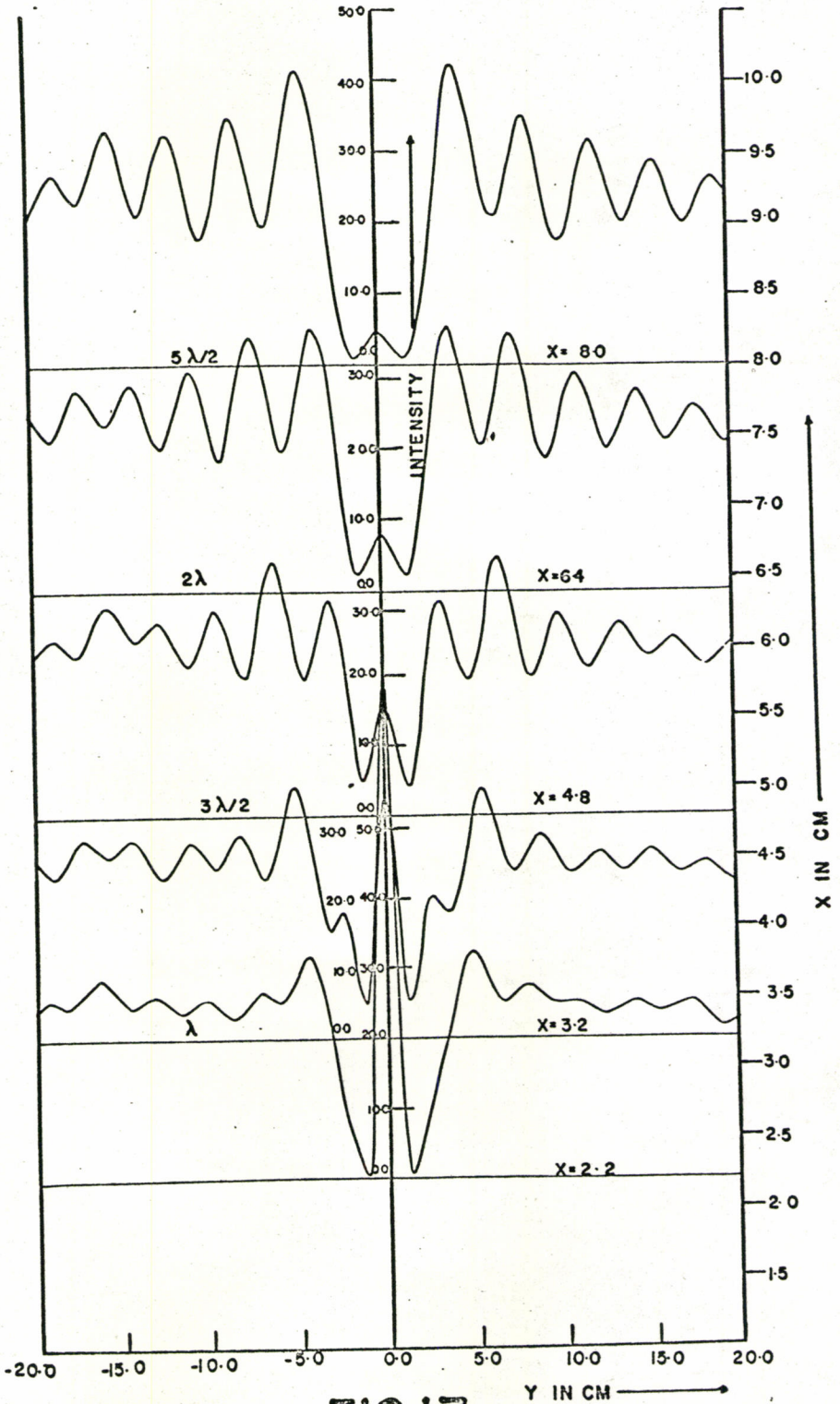

FIG·17

UNNORMALIZED DIFFRACTION PATTERNS

FOR 1·0 INCH LUCITE ROD

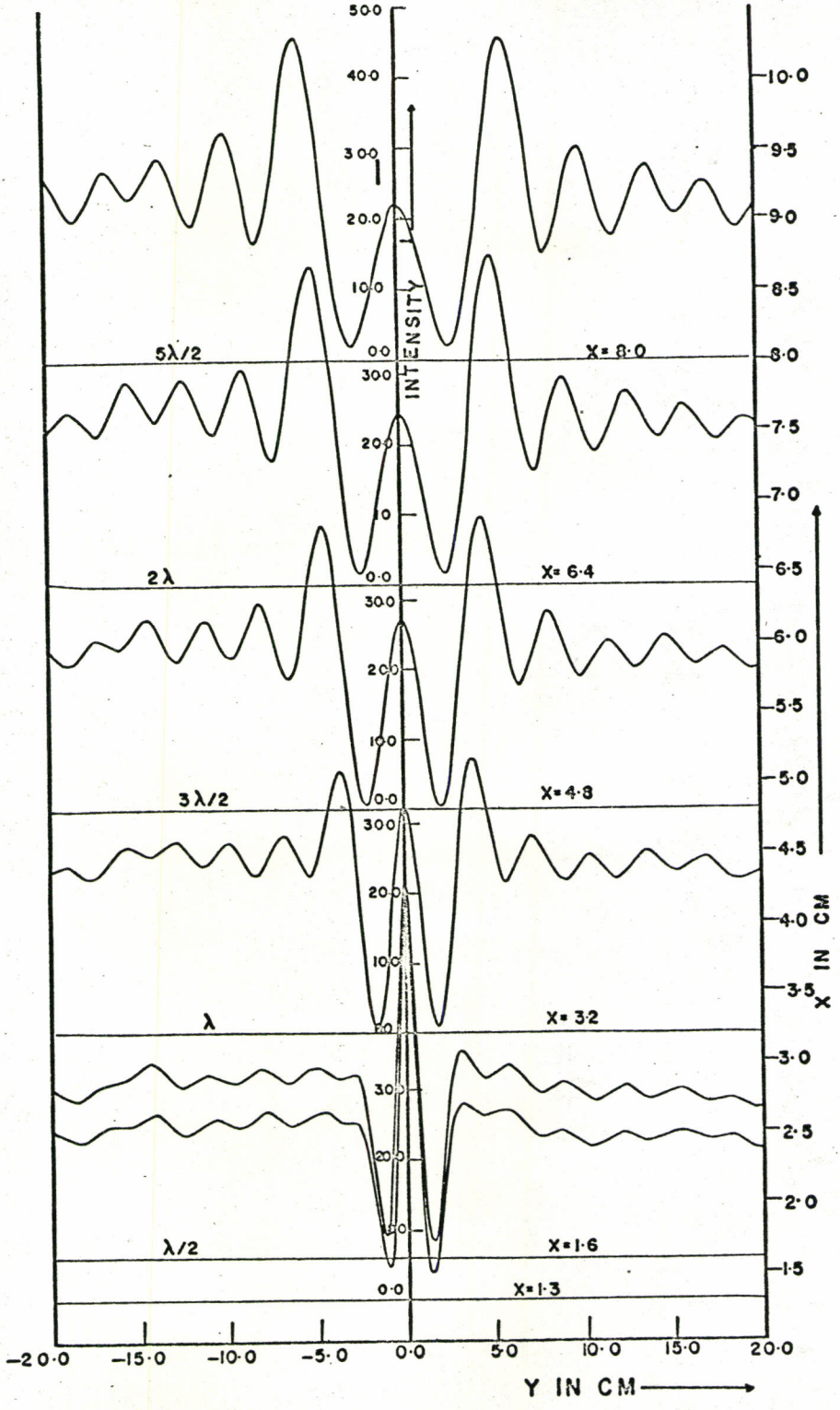

FIG·18

5-11 Normalized Fields for 1.5 inch and 1.0 inch Rods

Fig. 20 and Fig. 21 show the normalized diffraction fields along the X-axis. The continuous curve shows the experimental results while the dotted lines show the calculated results. The normalized fields are plotted along the vertical axis.

Here, also, there are discrepancies between the theoretical and calculated and experimental results. If we compare Fig. 20 and Fig. 21, we see that the diffraction pattern for the 1.5 inch rod starts with a higher peak and then falls off more rapidly than that of the 1.0 inch rod. This can also be seen in Fig. 17 and Fig. 18, where the central maxima fall off in the same fashion.

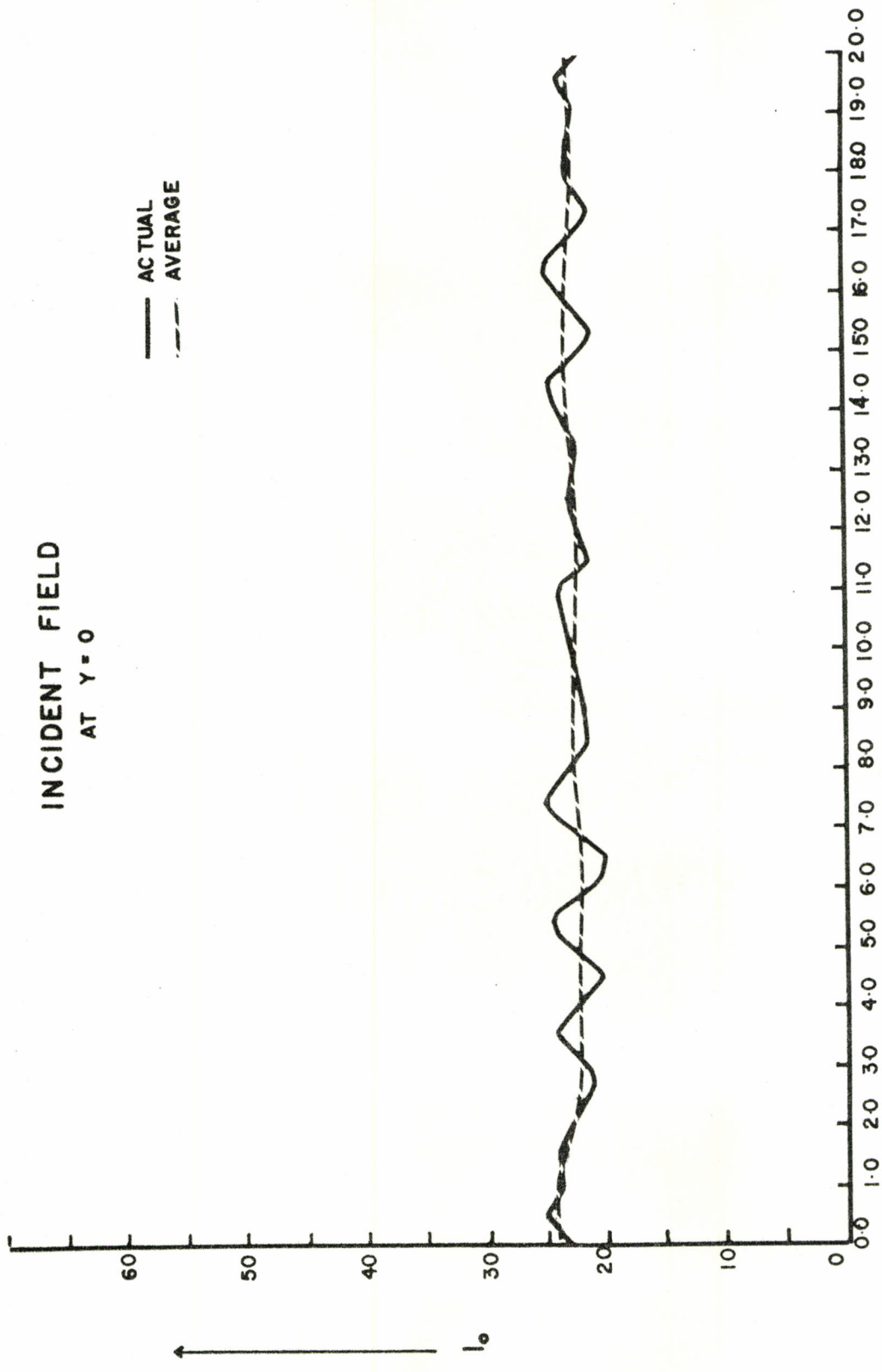
INCIDENT FIELD
AT Y = 0
ACTUAL
AVERAGE
I_o
60
50
40
30
20
10
0
0·0
1·0
2·0
3·0
4·0
5·0
6·0
7·0
8·0
9·0
10·0
11·0
12·0
13·0
14·0
15·0
16·0
17·0
18·0
19·0
20·0
X IN CM

FIG·19

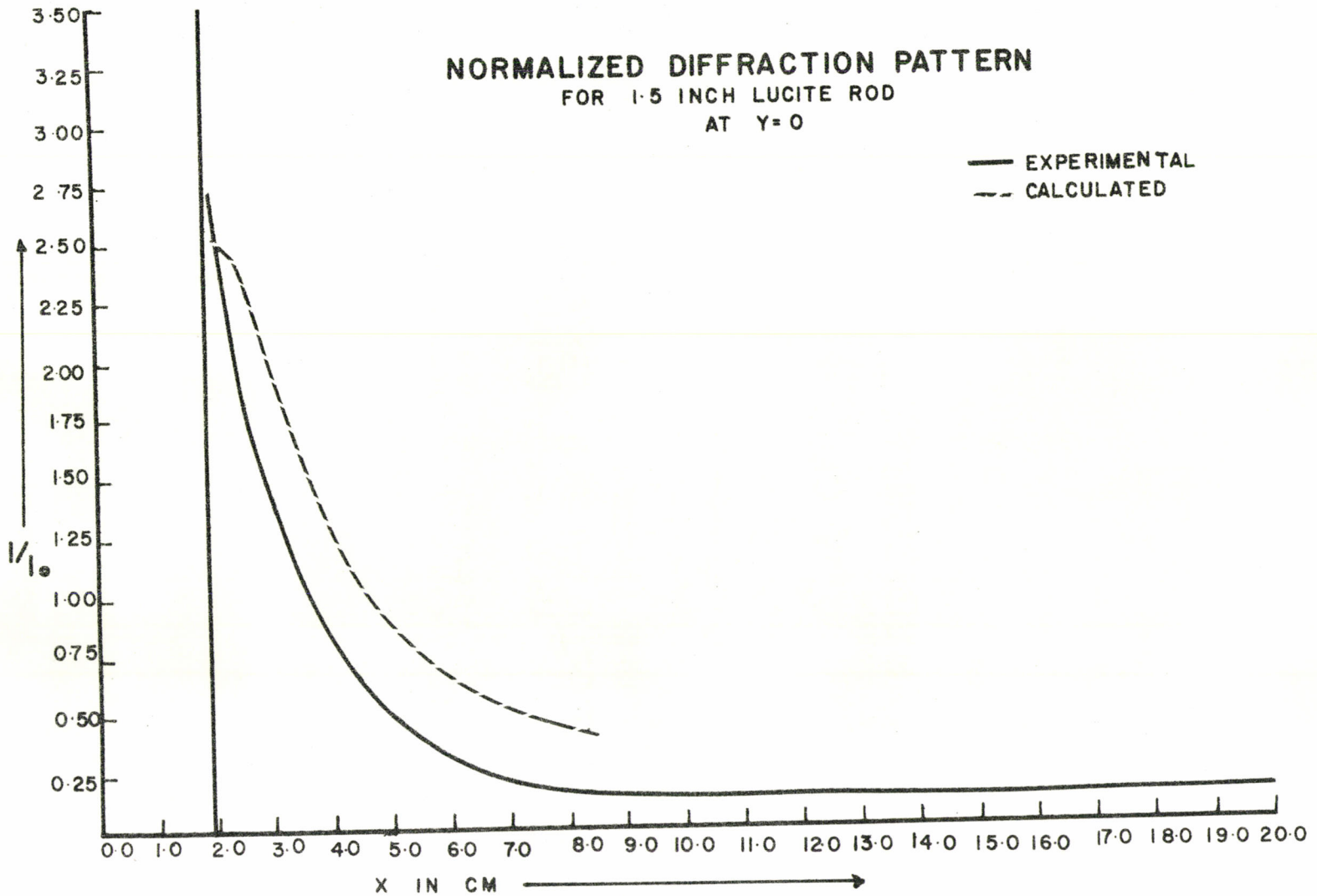
NORMALIZED DIFFRACTION PATTERN
FOR 1·5 INCH LUCITE ROD
AT Y= 0
EXPERIMENTAL
CALCULATED
3·50
3·25
3·00
2·75
2·50
2·25
2·00
1·75
1·50
1·25
1·00
0·75
0·50
0·25
I/I₀
0·0 1·0 2·0 3·0 4·0 5·0 6·0 7·0 8·0 9·0 10·0 11·0 12·0 13·0 14·0 15·0 16·0 17·0 18·0 19·0 20·0
X IN CM

FIG·20

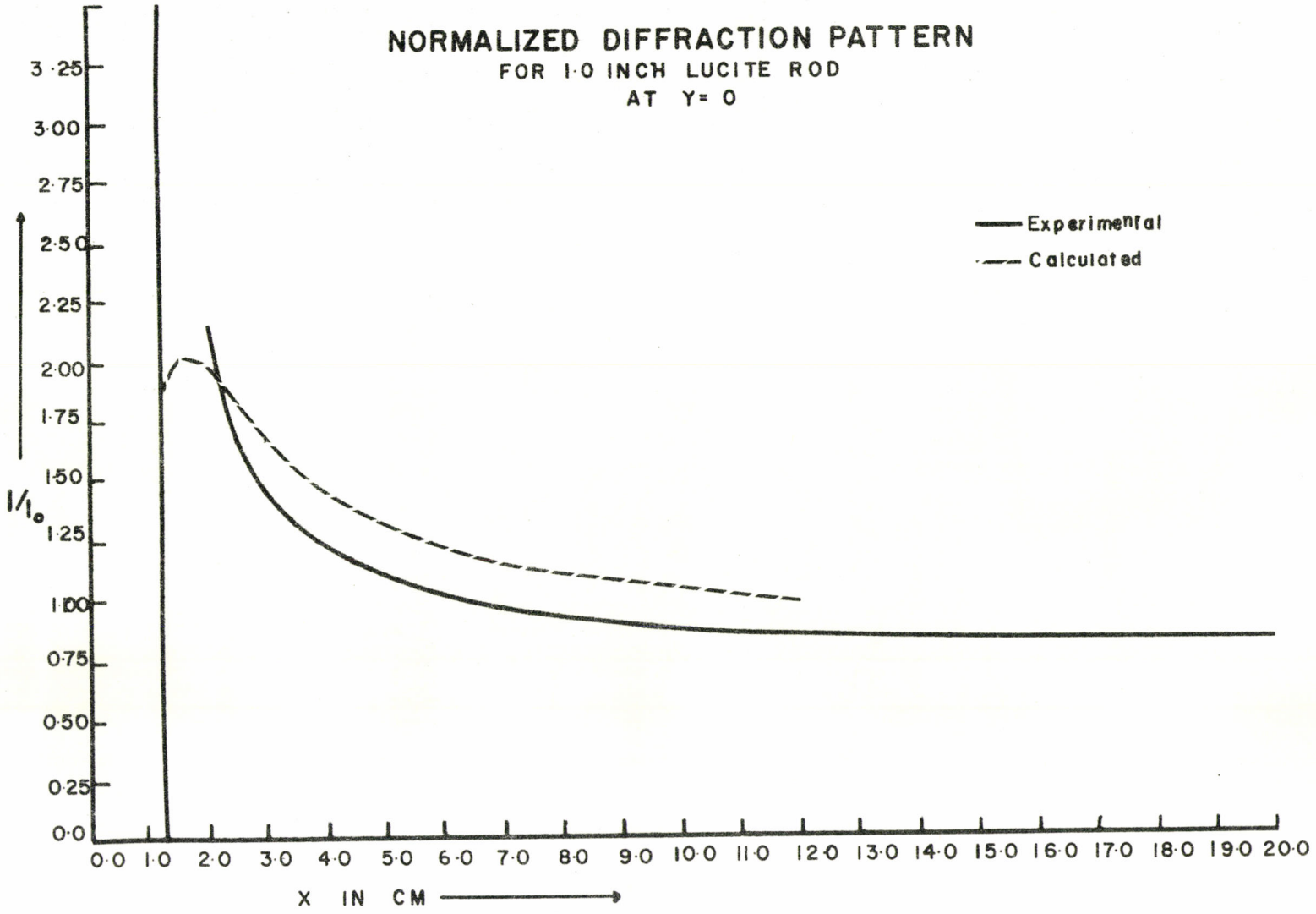
NORMALIZED DIFFRACTION PATTERN
FOR 1·0 INCH LUCITE ROD
AT Y= 0
Experimental
Calculated
I/I₀
3·25
3·00
2·75
2·50
2·25
2·00
1·75
1·50
1·25
1·00
0·75
0·50
0·25
0·0
0·0 1·0 2·0 3·0 4·0 5·0 6·0 7·0 8·0 9·0 10·0 11·0 12·0 13·0 14·0 15·0 16·0 17·0 18·0 19·0 20·0
X IN CM

FIG·21

CHAPTER 6

CONCLUSIONS

The main purpose of these experiments was to study the optical behaviour of the prisms and the dielectric rods at microwave frequencies. The standing wave patterns for prism A and prism B show the reflection properties of the prisms. The prism reflects a portion of the energy back into the waveguide and transmits the other portion through the prism into free space. The experiments show that the prism behaves as a dielectric waveguide and concentrates the wave at its tip by guiding it between its boundary walls. Therefore, the experiments with the prisms exhibit that the prisms behave as dielectric waveguides.

The behaviour of the prisms in these experiments could not be explained completely on the basis of simple optics only. The reason is that we can not assume that the field inside the waveguide is a simple plane wave. In fact, the field inside the waveguide is a superposition of two plane waves. Therefore, the simplified assumption of a critical reflection of a plane electromagnetic wave from a prism is not valid.

Probably, for this reason, the experiments with the prism could not establish the Goos-Häenchen shift inside the waveguide. What actually happens in the experiments is that the prism here acts in the

same fashion as prism A shown in Fig. 11 and Fig. 12. There, it can be seen that the prism has shifted the intensity patterns to the left. Therefore, the prism in Fig. 1(b) also shifts the energy from the centre of the waveguide towards the bottom thereby throwing most of the energy into arm (3) rather than into arm (2). For the second maximum at x = 6 cm in Fig. 13, it may be said that the reflection from the first face of the prism is such that the energy is thrown into arm (3) again.

For a complete understanding of the prism experiments, a rigorous mathematical treatment is necessary on the basis of electromagnetic theory. However, the mathematical treatment becomes very complicated. The experiments do show, nevertheless, some of the complex properties of prisms used inside and outside of waveguides.

The diffraction equations were known for the other experimental studies. The mathematical calculations for the diffraction of microwaves by dielectric cylindrical rods at x = 0 and y = 0 are simpler compared to the other x and y values. Calculations for these cases have been done and experimental and calculated results have been compared. Calculations for other values of x and y have not been done since they are complicated and extensive. However, the experimental results have been shown in Fig. 17 and Fig. 18 in the form of unnormalized diffraction patterns. In these figures, the general nature of the diffraction patterns can be seen and studied comparatively.

For the other two cases (x = 0 and y = 0), the experimental and theoretical calculated values are shown in Fig. 15, Fig. 16,

Fig. 20 and Fig. 21. It can be seen that there is a fairly good agreement between the results. The experimental results follow the general form of the theoretical curves. However, there are still discrepancies. It has been found, in general, that the perpendicular polarization case was difficult to investigate experimentally and, for this reason, studies with this polarization have not been done extensively in this laboratory. The discrepancies can be explained. To obtain a complete match between the experimental and theoretical results, the experiment should satisfy the following criteria:

(1) The physical size of the diode becomes very important. In the parallel polarizations, the diode is looked upon as a point detector. When the electric vector is parallel to the Z-axis of the rod, the diode is orientated such that its length is also parallel to the Z-axis. Now, if we look at the diode along the Z-axis, the diode appears as a point detector.

Now in the case of the perpendicular polarization, the diode is orientated so that it becomes perpendicular to the Z-axis of the rod. Therefore, if we look at the diode along the Z-axis, it no longer appears to be a point detector but has a definite finite length ($\lambda/2 = 1.6$ cm). An ideal situation for investigation of this polarization would be to obtain an approximate point detector. However, this is impractical

at this wavelength since such a detector would then be extremely insensitive.

(2) The experiment should satisfy the plane wave condition. Experimental conditions do not satisfy this condition completely. The wave coming from the horn is not a plane wave. To satisfy this condition to some extent, we have to go a long distance away from the horn and allow the wave to spread fast. In doing so, we are faced with the problem of reflections from the walls, ceiling and floor of the room plus the diffraction and scattering from all obstacles in its way. Although the microwave absorbers reduce these considerably, there is still some reflection from them.

(3) A perfect alignment of the experimental equipment has to be achieved. It is very essential that the diode is perfectly parallel to the X- or Y-axis, as the case may be, for taking the experimental runs. This can only be done by satisfying the conditions of perfect alignment on each and every interdependent step. Otherwise, since the scattered field is composed of both E_x and E_y components, the diode will pick up less of the one and a little of the other.

(4) The diode itself has to be perfectly symmetric. The diode should have a complete symmetry on either side of its centre. It has been found that the diode leads were not placed per-

fectly in line when it was manufactured. However, asymmetry may have occurred when the leads were cut off. On one side, the lead may be of a different length than on the other.

Within these limitations, the experiments on the perpendicular polarization do yield partially satisfactory agreement with the theory. Particularly, the finite detector effect is serious as can be seen by the general "washing out" of the pattern in Fig. 15 and Fig. 16.

APPENDIX

To find the value of the constant A_m, we apply the boundary conditions:

$$\underbrace{\left[(H_z)_{in} + (H_z)_{sc}\right]}_{\text{= outside the rod}}_{r=a} = \underbrace{\left[(H_z)\right]}_{\text{= inside the rod}}_{r=a} \tag{A.1}$$

and,

$$\underbrace{\left[\frac{\partial}{\partial r}(H_z)_{in} + \frac{\partial}{\partial r}(H_z)_{sc}\right]}_{\text{= outside the rod}}_{r=a} = \underbrace{\left[\frac{\partial}{\partial r}(H_z)\right]}_{\text{= inside the rod}}_{r=a} \tag{A.2}$$

From equation (2.5), the field outside the rod

$$\left[(H_z)_{in} + (H_z)_{sc}\right]_{r=a}$$

$$= H_o \sum_{m=0}^{\infty} C_m i^m \left[J_m(ka) + A_m H_m^{(1)}(ka)\right]\cos m\theta\Big|_{r=a} \tag{A.3}$$

Similarly, (H_z) inside the rod can be expressed,

$$(H_z) = H_o \sum_{m=0}^{\infty} C_m i^m B_m J_m(nka) \cos m\theta \tag{A.4}$$

Applying the boundary conditions (A.1) and (A.2) on (A.3) and (A.4), we get

$$\left.\begin{aligned} J_m(ka) + A_m H_m^{(1)}(ka) &= B_m J_m(nka) \\ J_m'(ka) + A_m H_m^{(1)'}(ka) &= \frac{1}{n} B_m J_m'(nka) \end{aligned}\right\} \tag{A.5}$$

which gives

$$A_m = \frac{\begin{vmatrix} -J_m(ka) & -J_m(nka) \\ -J_m'(ka) & -\frac{1}{n}J_m'(nka) \end{vmatrix}}{\begin{vmatrix} H_m^{(1)}(ka) & -J_m(nka) \\ H_m^{(1)'}(ka) & -\frac{1}{n}J_m'(nka) \end{vmatrix}}$$

$$= -\left[\frac{\frac{1}{n}J_m(ka)\,J_m'(nka) - J_m(nka)\,J_m'(ka)}{\frac{1}{n}H_m^{(1)}(ka)\,J_m'(nka) - J_m(nka)\,H_m^{(1)'}(ka)}\right] \qquad \text{(A.6)}$$

where,

$$\left.\begin{aligned} H_m^{(1)}(ka) &= J_m(ka) + i\,Y_m(ka) \\ H_m^{(1)'}(ka) &= J_m'(ka) + i\,Y_m'(ka) \end{aligned}\right\} \qquad \text{(A.7)}$$

$$\left.\begin{aligned} J_m'(ka) &= \tfrac{1}{2}\left[J_{m-1}(ka) - J_{m+1}(ka)\right] && m \neq 0 \\ J_o'(ka) &= -J_1(ka) && m = 0 \end{aligned}\right\} \qquad \text{(A.8)}$$

$$\left.\begin{aligned} Y_m'(ka) &= \tfrac{1}{2}\left[Y_{m-1}(ka) - Y_{m+1}(ka)\right] && m \neq 0 \\ Y_o'(ka) &= -Y_1(ka) && m = 0 \end{aligned}\right\} \qquad \text{(A.9)}$$

Substituting (A.7), (A.8) and (A.9) in (A.6), we get

$$A_m = -\left[\frac{1}{n} J_m(ka) J'_m(nka) - J'_m(ka) J_m(nka)\right]$$

$$x\left\{\frac{\left[\frac{1}{n} J_m(ka)J'_m(nka) - J'_m(ka)J_m(nka)\right] - i\left[\frac{1}{n} J'_m(nka)Y_m(ka) - Y'_m(ka)J_m(nka)\right]}{\left[\frac{1}{n}J'_m(nka)Y_m(ka) - Y'_m(ka)J_m(nka)\right]^2 + \left[\frac{1}{n} J'_m(nka)J_m(ka) - J'_m(ka)J_m(nka)\right]^2}\right\}$$

(A.10)

Now, the component E_y of the electric vector is related to H_z by,

$$(E_y)_{sc} = \frac{1}{i\omega\epsilon_o} \frac{\partial}{\partial x} (H_z)_{sc}$$

$$(E_y)_o = \frac{1}{i\omega\epsilon_o} \frac{\partial}{\partial x} (H_z)_o \qquad \text{(A.11)}$$

$$\left(\frac{E_y}{E_o}\right)_{\text{normalized}} = \frac{\frac{1}{i\omega\epsilon_o} \frac{\partial H_z}{\partial x}}{\frac{1}{i\omega\epsilon_o} x \frac{\partial H_z}{\partial x}} = \frac{\frac{\partial}{\partial x} H_z}{H_o \frac{\partial}{\partial x}(e^{ikx})}$$

$$= \frac{1}{ik}\left[\frac{\partial}{\partial x}\left[\frac{H_z}{(H_z)_o}\right]\right] \qquad \text{(A.12)}$$

Now, $x = r \cos\theta$

$$\frac{\partial}{\partial x} = \cos\theta \frac{\partial}{\partial r} - \frac{\sin\theta}{r} \frac{\partial}{\partial \theta} \qquad \text{(A.13)}$$

Therefore, we get

$$\left(\frac{E_y}{E_o}\right)_{\text{normalized}} = \frac{1}{ik} \sum_{m=0}^{\infty} C_m i^m A_m \cos\theta \cos m\theta \, k H_m^{(1)'}(kr)$$

$$+ \sum_{m=0}^{\infty} C_m i^m A_m \frac{\sin\theta}{r} H_m^{(1)}(kr) \, m \sin m\theta \qquad \text{(A.14)}$$

$$= \sum_{m=0}^{\infty} C_m i^{m-1} A_m F_m(r,\theta)$$

where,

$$F_m(r,\theta) = \cos m\theta \cos\theta H_m^{(1)'}(kr) + \frac{m \sin m\theta \sin\theta H_m^{(1)}(kr)}{kr} \qquad (A.15)$$

The values of A_m and F_m are found from (A.10) and (A.15) respectively, which, when substituted in (A.14), give the calculated amplitudes and, hence, the intensities of the diffraction paterns for a cylindrical rod.

REFERENCES

NO.

1. Dignum, R., "Dielectric Constant Measurements and also Microwave Optics of a Prism", 1960, M.Sc. Thesis, McMaster University.

2. Froese, C., and Wait, J. R., "Calculated Diffraction Patterns of Dielectric Rods at Centimetric Wavelengths", 1954, Can. J. Phys., 32, 775.

3. Ginzton, E. L., "Microwave Measurements", 1957, McGraw-Hill.

4. Goos, F., and Haenchen, H., 1947, Ann. Physik, 1, 333.

5. Hedgecock, N. E., "Microwave Optics of a Prism", 1959, Ph.D. Thesis, McMaster University.

6. Hedgecock, N. E., and McLay, A. B., "Diffraction of Nearly Plane 3.2 CM EM Waves by 45° and 90° Conducting Wedges — Comparison with Theory", 1959, IRE Trans., Dec., AP-7, S 284.

7. Jordan, C. E., and McLay, A. B., "Diffraction of 3.2 CM Electromagnetic Waves by Dielectric Rods", 1957, Can. J. Phys., 35, 1253.

8. Jordan, C. E., "Total Reflection of Microwaves by a Prism and Semi-cylinder", 1960, M.Sc. Thesis, McMaster University.

9. Keys, J. E., "Diffraction of Microwaves", 1953, M.Sc. Thesis, McMaster University.

10. King. R. W. P., and Wu, T. T., "The Scattering and Diffraction of Waves", 1959, Harvard University Press, Camb., Mass.

11. Kodis, R. D., "An Experimental Investigation of Microwave Diffraction", 1952, J. Appl. Phys., 23, 249.

12. Kneeland, D. R., "Reflection and Total Reflection of Microwaves by Prism", 1954, M.Sc. Thesis, McMaster University.

13. Leung, P., "Microwave Optics of a Prism", 1961, M.Sc. Thesis, McMaster University.

14. McLay, D. B., "Diffraction of Microwaves by Conducting Rods", 1951, M.Sc. Thesis, McMaster University.

15. Montgomery, C. G., "Microwave Measurements", 1947, Rad. Lab. Series No. 11, McGraw-Hill.

16. Proc. of the Syonposium, "Modern Advances in Microwave Techniques", 1954, Poly. Tech. Inst., Brooklyn, Vol. IV, Nov.

17. Renard, R. H., "Total Reflection : A New Evaluation of the Goos-Haenchen Shift", 1964, J. Opt. Soc. Am., No. 10, 54, 1190.

18. Slatter, J. C., "Microwave Transmission", 1942, Mc-Graw-Hill, N.Y.

19. Southworth, G. C., "Principles and Applications of Waveguide Transmission", 1956, D. Van Nostrand Co., N.Y.

20. Subbarao, M. K., and McLay, A. B., "Diffraction of 3.2 CM Electromagnetic Waves by Dielectric Rods", 1956, Can. J. Phys., 34, 546.

21. Subbarao, M. K., and McLay, A. B., "Diffraction of 3.2 CM Electromagnetic Waves by Dielectric Rods", 1956, Can. J. Phys., 34, 555.

22. Tremblay, R., and Boivin, A., "Concepts and Techniques of Microwave Optics", 1966, Appl. Opt., Feb., 245.

23. Twersky, V., "Microwaves and Optics", 1965, Appl. Opt., Oct., 1213.

24. Weeks, W. L., "Electromagnetic Theory for Engineering Applications", 1964, John Wiley & Sons, N.Y.

25. Wiles, S. T., and McLay, A. B., "Diffraction of 3.2 CM Electromagnetic Waves by Cylindrical Objects", 1954, Can. J. Phys., 32, 372.

26. Young, W. A., "Diffraction of Microwaves Along the Axis of Propagation Behind Conducting and Dielectric Rods and a Plastic Prism", 1963, M.Sc. Thesis, McMaster University.